Intraoperative navigation and intraoperative CT in orthopaedic oncology surgery

R.P.J. van den Ende
Master Thesis Technical Medicine
Medical Imaging & Interventions
September 2015

UNIVERSITY OF TWENTE.

Leiden University Medical Center

Exam committee members

Chairman	Prof. dr. ir. C.H. Slump[1]
Clinical supervisor	Dr. P.D.S. Dijkstra[2]
Technical supervisor, LUMC	Dr. B.C. Stoel[3]
Technical supervisor, LUMC	Dr. ir. B.L. Kaptein[4]
Technical supervisor, UT	Prof. dr. ir. C.H. Slump[1]
External member	Dr. ir. F. van der Heijden[1]
Tutor	Drs. N.S. Cramer Bornemann[5]

[1]MIRA Institute for Biomedical Technology and Technical Medicine, University of Twente, Enschede, The Netherlands

[2]Department of Orthopaedic Surgery, Leiden University Medical Center, Leiden, The Netherlands

[3]Division of Image Processing, Department of Radiology, Leiden University Medical Center, Leiden, The Netherlands

[4]Biomechanics and Imaging Group, Department of Orthopaedics, Leiden University Medical Center, Leiden, The Netherlands

[5]School of Technical Medicine, University of Twente, Enschede, The Netherlands

i. Preface

The work in this thesis has been performed at the Leiden University Center, department of Radiology, division of Image Processing, in collaboration with the department of Orthopaedic Surgery. It was submitted in partial fulfillment of the requirements of the Master of Science degree in Technical Medicine.

I started this graduation project in October 2014, simultaneously with the introduction of an intraoperative CT scanner in orthopaedic oncology surgery in the LUMC. During this project, I witnessed the challenges involved in the implementation of a new technique. I enjoyed the close collaboration with the Department of Radiology, Department of Orthopaedic Surgery and BrainLAB in solving these challenges and exploiting the new possibilities.

I would like thank my clinical supervisor, Sander Dijkstra, for his clinical guidance and his support in helping me understand the principles of surgical management of primary bone tumors.
I would also like to thank my technical supervisors, Bart Kaptein, Berend Stoel and Kees Slump, for their guidance, structural feedback and interesting discussions.
Last but not least, I would like to thank Nicole Cramer Bornemann for her support as a tutor.

Leiden, August 25, 2015
Roy van den Ende

ii. Summary

Bone sarcomas are treated by surgical resection with subsequent bone reconstruction. In these surgeries in the LUMC, an intraoperative navigation system is used in which recently a mobile intraoperative CT scanner was integrated for use in the operation room (OR). Although the navigation system is designed for use in brain and spine surgery, in the LUMC it also used in orthopaedic oncology surgery of the pelvis and the extremities.

One of the options for reconstructing a bone defect created by a tumor resection is using an allograft. It is cut to the desired shape in order to fit in the bone defect and subsequently secured with screws. Currently, shaping the allograft is completely based on the surgeon's skills by using a ruler and visual interpretation (called: freehand method). Navigated allograft reconstruction has been described in literature but in those studies the preoperative tumor resection planning was also used as the allograft reconstruction planning. When the resection planning is not performed perfectly or the surgeon had to deviate from planning, the tumor resection planning will not be valid for allograft reconstruction. Alternatively, using an intraoperative CT scanner, the bone defect can be scanned and based on that CT scan an allograft reconstruction planning can be made. However, this is not yet implemented in clinical practice in the LUMC.

The aim of this thesis was 1) to perform a pilot phantom study on navigated allograft reconstruction as a first step in ultimately achieving intraoperative CT based navigated allograft reconstruction and to compare this method to the currently used freehand method and 2) to perform a clinical evaluation of the use of the intraoperative CT scanner in orthopaedic oncology surgery.

In the pilot phantom study, a hemicortical lateral distal femur resection was performed in two femur Sawbones, based on the case of an actual patient that was treated in the LUMC. For each bone defect, three conventional freehand reconstructions and three navigated reconstructions were performed using femur Sawbones. The reconstruction planning for the navigated reconstructions was made from an intraoperative CT scan of the bone defect. Allograft fit was assessed by determining cortex gap volume between host and allograft. Mean gap volume for the freehand reconstructions was 3385 mm^3 compared to 2191 mm^3 for the navigated reconstructions ($p=0.01$).

In the pilot phantom study, navigated allograft reconstruction using a reconstruction planning made from an intraoperative CT scan of the bone defect led to smaller and more consistent cortex gap volumes compared to conventional freehand allograft reconstruction. Implementation of this technique in clinical practice is expected to increase allograft fit, but additional challenges have to be solved to accomplish this, including preoperative scanning of the allograft, (semi-)automatic image registration of the allograft with patient bone and (semi-)automatic intraoperative segmentation of the bone defect.

Experiences with the intraoperative CT scanner during this graduation project have shown that the intraoperative CT scanner is a substantial improvement for orthopaedic oncology surgery. Main advantages were 1) easy, accurate registration on any anatomy, 2) visualizing the actual intraoperative anatomy and 3) intraoperative 3D imaging (e.g. to accurately verify screw positions).

iii. Table of contents

1 Introduction

1.1 Clinical context

Patients with a primary bone tumor eligible for operative treatment are treated by resection of the tumor and subsequent reconstruction using an autograft, allograft, endoprosthesis or a combination of those. At the LUMC, a commercially available navigation system is available for use for the resection of a bone tumor and/or placement of screws (Curve; BrainLAB, Feldkirchen, Germany). The navigation system is aimed at providing the surgeon with patient image data on which the surgical tools are visualized real-time. It is comparable to a car navigation system which shows your location with respect to the map. The intraoperative navigation is accomplished by markers that are attached to the treated bone of the patient and the surgical tools. The markers are tracked by an infrared camera. The navigation system is originally developed for brain surgery, and over the last twenty years also for spine surgery. However, at the LUMC it is also used for the resection of bone tumors in the pelvic area and the extremities.

Imaging preparation for this orthopedic oncology surgery consists of a preoperative CT and MRI scan. The CT scan provides information regarding the bone structures, while the MRI scan provides information regarding the tumor (soft tissue). The tumor is segmented in the MRI scan in order to plan the operation and image registration is performed to align the MRI and CT scan. Image registration and surgical planning is performed using dedicated planning software (iPlan; BrainLAB, Feldkirchen, Germany).

Before a navigated operation procedure can be started, patient anatomy needs be registered to the preoperative image data. This can be accomplished by using paired point matching, surface matching, or fluoro-CT matching. However, using this, the surgeon is always navigating using preoperative data. If the anatomy of the patient changes, e.g. because of a resection, this is not reflected in the image data. To provide the surgeon with up-to-date imaging, a mobile intraoperative CT scanner (Airo; Mobius Imaging, Ayer, Massachusetts) was integrated with the Curve navigation system. The Airo CT scanner can provide the surgeon with image data of the intraoperative situation. Markers on the gantry of the CT scanner allow for a quick registration procedure.

The application of a navigation system in orthopaedic oncology surgery is reported to aid in achieving adequate margins and increasing osteotomy accuracy [1]–[12]. One of the options for reconstructing a bone defect created by a tumor resection is using an allograft. Allograft is donated bone from another human being. The allograft is cut to the desired shape in order to fit in the bone defect and subsequently secured with screws. Currently, this is completely based on the surgeon’s skills by using a ruler and visual interpretation. However, the navigation system can also aid in the reconstruction of the bone defect using an allograft. Navigated reconstruction of an allograft using the same planning that was used for the tumor resection, in combination with the improved osteotomy accuracy is reported to improve allograft fit [5], [13], [14].

1.2 Research purposes

The introduction of the mobile intraoperative CT scanner creates new possibilities in the field of orthopaedic oncology surgery. Studies that describe navigated reconstruction of an allograft using navigation use the preoperative tumor resection planning also for allograft reconstruction. In theory, the allograft should then fit perfectly in the bone defect. In practice, however, the planning is not always performed exactly as planned. Additionally, a bone tumor can progressively destruct the bone, even after preoperative imaging was acquired, which could have implications on the performed surgery. If the surgeon had to deviate from planning, the preoperative plan will not be valid for allograft reconstruction. The Airo CT scanner can provide the surgeon with image data on the created bone defect. If a surgical planning for the reconstruction can be made from this image data, the allograft can be reconstructed using the actual geometry of the bone defect, rather than relying on preoperative imaging.

The first study aim was to perform a pilot phantom study on navigated allograft reconstruction as a first step in ultimately achieving intraoperative CT based navigated allograft reconstruction of the created bone defect and to compare this method to the currently used freehand method.

The introduction of a new technique like this has consequences for the OR workflow and as with any new technique, teething problems may occur. Therefore, the second study aim was to perform a clinical evaluation of the use of the intraoperative CT scanner in orthopaedic oncology surgery. The surgical workflow using the intraoperative CT scanner is compared with the workflow of conventional navigated operation procedures. Common problems/challenges encountered in the OR are discussed. Additionally, it is discussed whether a navigated procedure in combination with the Airo CT scanner is a substantial improvement for orthopaedic oncology surgery over the conventional navigation procedures.

The mentioned study aims can be translated into two research questions:

1. Does navigated allograft reconstruction using a reconstruction planning from intraoperative CT lead to more accurate reconstruction compared to freehand allograft reconstruction?
2. Is the new intraoperative CT scanner a substantial improvement for orthopaedic oncology surgery, a discipline for which it was not specifically designed?

1.3 Thesis outline

This chapter contains the clinical context, the purpose of this research and a short description of the performed work. Chapter 2 contains the theoretical background of various subjects involved in this thesis and a review of the published literature. Chapter 3 contains a case report which describes the first joint-saving resection of a bone sarcoma using the navigation system in combination with the intraoperative CT scanner in the LUMC. Chapter 4 contains an article that was written about the pilot phantom study we have performed regarding intraoperative CT based navigated allograft reconstruction. Chapter 5 contains a clinical evaluation of the use of the intraoperative CT scanner in orthopaedic oncology surgery. Chapter 6 summarizes the main findings of this thesis and Chapter 7 states recommendations for future research.

2 Background

2.1 Primary bone tumors

Primary bone tumors are rare and the majority of the primary bone tumors is benign. The exact incidence of benign tumors is difficult to determine, since most are non-symptomatic [15]. On the contrary, the incidence of malignant primary bone tumors is well documented. Approximately only 0.2% of all malignancies are bone sarcoma. Common primary malignant bone tumors are osteosarcoma, chondrosarcoma and Ewing sarcoma, making up for more than 75% of all primary malignant bone tumors [16], [17].

Osteosarcoma is most common at the age of 10-25 and over 50 years. It is mostly found in the metaphysis of the long extremity bones (femur, tibia and humerus), especially around the knee [18]. Chondrosarcoma is most seen in 40-70 year olds. It commonly arises from pre-existing bony lesions such as enchondromas or osteochondromas. Common locations for chondrosarcoma are the pelvis, ribs, ilium, femur and humerus.
About 80% of Ewing sarcoma is found in patients under 20 years old. It is rare in patients older than 30. It is mostly found in the diaphysis or diaphyseal-metaphyseal portion of the long bones, pelvis and ribs.

Early symptoms of malignant bone tumors include non-specific pain around a joint, not related to activity or weight bearing. Later symptoms include swelling, restriction of movement of the limb and pain related to activity or weight bearing. About 20% of patients present with a pathological fracture induced by the bone tumor or an incidental finding of a suspicious bone lesion on radiographs taken for other reasons [16].

When suspicion of a new bone lesion has risen, further investigation has to be performed for identification of the lesion. Initial investigations include X-rays of the entire bone, including the joints connected to the suspected bone. A MRI is performed to analyze bone lesion characteristics and involvement of soft tissue and joints, since MRI provides excellent soft tissue imaging [19]. Among other MRI protocols, a dynamic gadolinium enhanced MRI scan is obtained in order to assess various parameters, such as slope, wash out and interval between start of enhancement of artery and of lesion. Different types of tumors result in different values for these parameters [20]. If the MRI indicates a risk of a malignant bone tumor, a biopsy is mandatory. After definitive diagnosis, systemic staging is performed, evaluating systemic spread of the tumor.

Systemic staging involves a PET CT scan or bone scan and a CT scan of the chest to assess the presence of a primary tumor or metastases.

2.1.1 Tumor resection

Excision of a bone tumor consists of two main parts: surgical excision of the tumor and subsequent reconstruction of the created bone defect. Different surgical techniques can be used and important factors in the decision for the appropriate technique include tumor type, local and systemic staging, localization, patient age and patient choice.

In the past, amputation was a common method to resect primary malignant bone tumors. Amputation is, for patients, a hard to accept treatment. Advances in chemotherapy and imaging techniques has allowed for limb-salvage surgery [21]. Improved imaging allowed the surgeon to more accurately study the extent of the tumor, thereby preventing the need for amputation. The most important task in performing a limb-salvage procedure is resecting the bone tumor while maintaining adequate margins. A margin is defined adequate if it results in an acceptably low local recurrence rate. Different types of margins are defined (Fig. 1):

- Radical
- Wide
- Marginal
- Intralesional

A radical margin is achieved if the surgeon excises the entire bony compartment in which the tumor is located (e.g. the whole femur in Fig. 1). A wide margin is achieved when the surgeon cuts both around the tumor tissue and the reactive tissue, called the reactive zone, effectively cutting through healthy tissue in order to resect the tumor. A margin is marginal when the surgeon cuts around the tumor but cuts through the reactive zone. An intralesional margin is defined when the tumor is incised during surgery.

The treatment for benign bone tumors is in majority expectative; no treatment is given if the tumor is non-symptomatic. Aggressive benign tumors are preferably treated by curettage, which is the resection of the tumor by scraping the tumor tissue from or out of the bone (thereby achieving an intralesional resection margin). The advantage of this type of surgery is that it limits intraoperative and secondary reconstructive complications. Because bone stability is mostly preserved, reconstruction of the bone is only for filling the defect instead of mechanical support. Curettage can be followed by additional treatments by means of phenol or cryosurgery [22], [23]. The treatment for bone sarcoma consists of surgery (if appropriate when taking into account any metastasis) and neo-adjuvant and/or adjuvant therapy by means of chemotherapy and/or radiotherapy. The combination of additional treatments next to surgery depends on the type of malignant bone tumor.

Treatment for osteosarcoma includes surgery and neo-adjuvant and adjuvant chemotherapy. Modern surgical techniques allow limb-salvage surgery to be performed more often, thereby reducing amputation rates. Neoadjuvant and adjuvant therapy is given to reduce or destroy the

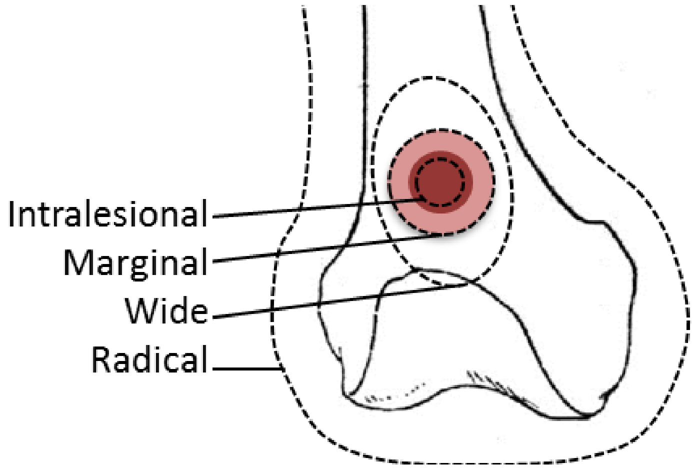

Figure 1. Different surgical margins in the resection of a bone tumor. The bone tumor is displayed in red with a pink reactive zone around it.

primary tumor and/or (micro)metastases. Radiotherapy is rarely used [16].
Chondrosarcoma is highly resistant to chemotherapy and radiotherapy. Despite of that, chemotherapy is still used to treat metastatic spread. Surgical resection is the principal treatment modality [16]. A wide excision has to be used in intermediate and high grade chondrosarcoma's. For low grade chondrosarcoma's, curettage is used more often.
Ewing sarcoma is sensitive to chemotherapy, radiotherapy and surgery. Neoadjuvant chemotherapy is important to treat metastases, which are often seen with Ewing sarcoma.

For more extensive reading about the described bone tumors and their respective treatments and other types of bone tumors, the reader is referred to [15], [16], [24].

2.1.2 Bone defect reconstruction

After resecting the tumor while maintaining adequate margins, reconstruction of the bone defect is required. This can be achieved using prostheses, autograft bone or allograft bone. The type of reconstruction depends on the diagnosis, size and location of the bone defect, involvement of other structures such as ligaments, tendons and muscles, treatment course, patient age, and patient choice.

As primary bone tumors frequently arise near joints, resection of the joint might be necessary. Reconstruction of the joint can be performed using an intra-articular allograft, an allograft-prosthetic composite or an endoprosthesis. An endoprosthesis is considered the gold standard. It consists of a stem that is inserted in the bone and connected to a prosthesis body, which is in turn connected to an articular device. This device is connected to a stem that is inserted in the bone opposite of the joint. Although an endoprosthesis is considered the gold standard, literature describes relatively high revision rates caused by infection, loosening and component wear, with 50-80% survival of endoprosthesis after 10 years [26], [27]. An endoprosthesis is therefore less suited for young patients, since it would require several revisions throughout his or her lifetime. Sparing the joint is therefore preferred and it is the recommended approach when considering functional outcome [25].

Autografts can be used for reconstruction but require long non-weight or partial weight bearing periods until complete union is achieved [28]. Next to that, autografts come with the risk of donor-site morbidity. Intercalary allografts provide superior initial stability but literature describes high rates of failure because of non-union, pathological fracture and infection [29]. Performing a hemicortical resection, thereby preserving continuity of the cortex, followed by inlay allograft reconstruction is reported to result in lower complication rates [30]. A hemicortical resection with subsequent inlay allograft reconstruction can provide a durable reconstruction, if it survives the first three years [31]. However, it is not recommended for high-grade bone lesions because of the higher risk of local recurrence, due to the difficulty in obtaining adequate margins. Performing hemicortical resections in high-grade tumors may be more successful if margins can be accurately maintained. Maintaining adequate margins can frequently be achieved in the case of diaphyseal resections, but becomes more complicated in metaphyseal or epiphyseal resections due to the morphology (Fig. 2).

Allografts are harvested under sterile conditions and subsequently stored at -80°C. They are then transported to a processing facility which prepares the grafts for implantation. Depending on the facility, additional sterilization is either not performed or performed with low-dose gamma radiation. After processing, the allografts are stored in a tissue bank at -80°C. Several measurements are performed by the processing facility to describe the morphology of the allograft. When an allograft is needed, the same measurements are performed on acquired radiographs of the patient bone and based on that, the best matching allograft is chosen. During surgery, the allograft is thawed in saline solution with antibiotics. When the bone defect is created after resection of the tumor, the allograft is cut to the desired shape to fit the bone defect using an oscillating saw. The allograft is placed under compression and fixated using titanium screws and, if necessary, a titanium plate.

Successful allograft incorporation is determined by several factors including surface contact area between the allograft and the recipient bone [32]. Remaining gaps between the cortexes of the allograft bone and patient bone are filled with spongiosa. However, no gaps are preferred. Cutting an allograft bone to the desired shape is challenging in the case of a hemicortical resection, especially in methaphyseal and epiphyseal resections were the anatomy is more complex compared to diaphyseal resections. Next to that, the allograft bone is never an exact match of the patient bone, making reconstruction for a proper fit more difficult.

Thus, performing a safe hemicortical resection in both low to intermediate and high-grade tumors with a subsequent durable reconstruction consists of two main goals:

1. Accurately maintaining adequate margins
2. Inlay allograft reconstruction and placement with superior fit.

The use of intraoperative navigation and the recently introduced mobile intraoperative CT scanner can aid in achieving these two main goals. A description of these techniques is given in section 3.2.

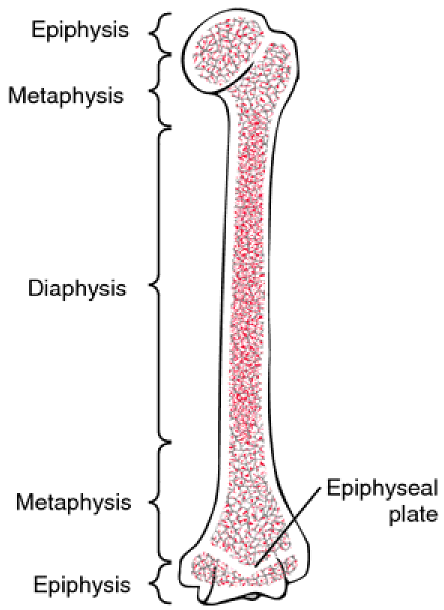

Figure 2: Structure of a long bone

2.2 Intraoperative navigation

The use of imaging techniques has allowed for preoperative evaluation of the anatomy and pathology of the patient. It is required that the surgeon transfers this information to the operation room in order to correctly perform the operation. To aid the surgeon, screens are placed in the OR which display the preoperative imaging. However, the surgeon would still have to make a translation from the imaging as seen on the computer screens to the patient which is operated on. This can be challenging, especially in the case of complex anatomy. Therefore, it would be even more helpful to have a real time visualization of the anatomy of the patient combined with the position and orientation of the used objects/tools. To accomplish this, numerous navigation systems have been introduced for use in the operating room. Its goal is to provide the surgeon accurate information regarding the anatomy of the patient and the position of the surgical tools with respect to the patient [33], [34]. The image data is generally provided by preoperative imaging of the patient. Intraoperative navigation is used in several disciplines, including neurosurgery, ear, nose and throat surgery and orthopaedic surgery [35].

2.2.1 Navigation system components

The navigation system used in the LUMC consists of a computer workstation (Curve; BrainLAB, Feldkirchen, Germany) with two touch screen monitors, which show the image data and surgical tools and allow user interaction. An infrared camera monitors the position of the patient and the surgical tools. To accomplish this, tracking bodies with small reflective spheres are attached to the patient and the surgical tools (Fig. 3). The patient tracking body (called: reference array) is attached to the patient bone using a clamp or screws on a location that has a fixed anatomical relationship with the target area. The tracking camera emits infrared light which is reflected by the spheres. From this reflection the position and orientation of the tracking bodies is measured.

Figure 3: Surgical tools and the clamp-style patient reference array with attached reflective markers for navigation purposes.

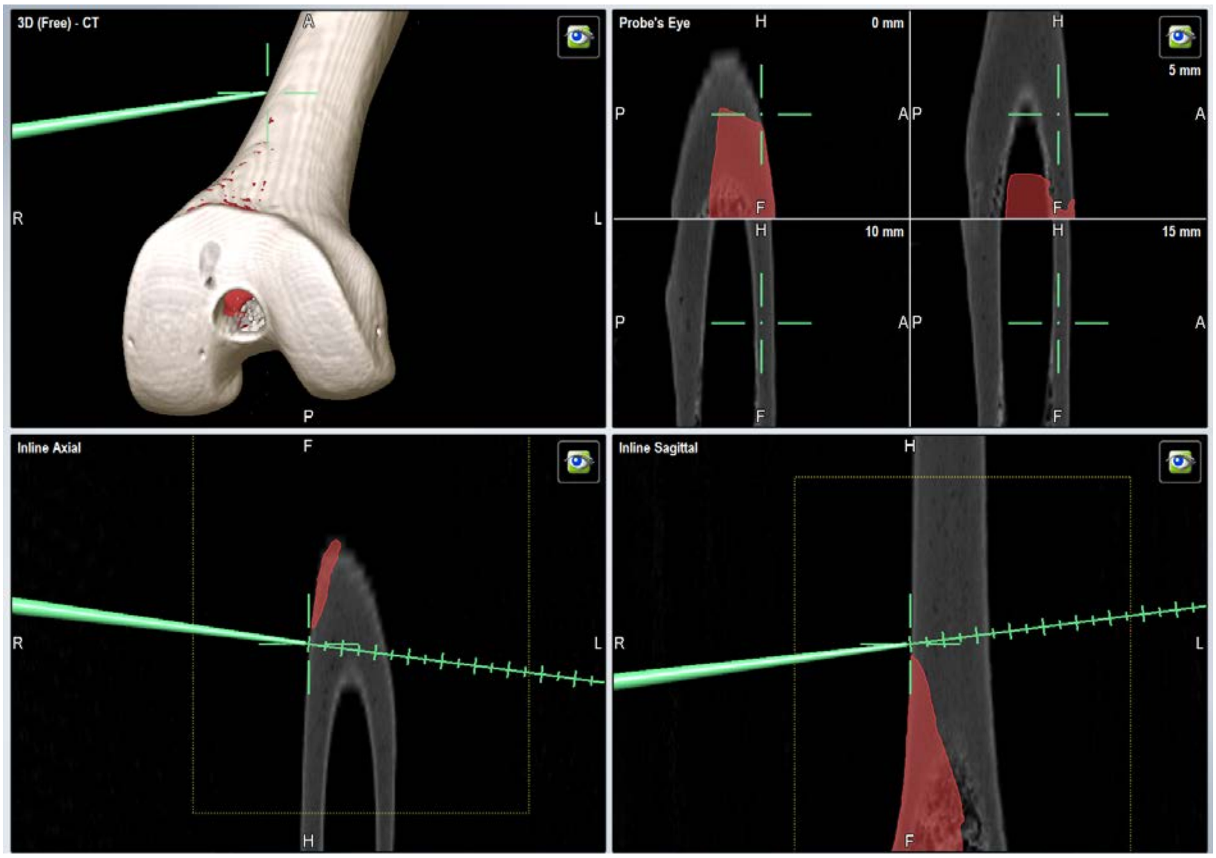

Figure 4: The pointer tool visualized over the image data. In the upper left corner a 3D visualization is shown. In the upper right corner the tip of the pointer is visualized, with increasing depth for each sub image. The lower left and lower right image show axial and sagittal view, respectively. Note that the axial and sagittal views provide an inline cross section with respect to the pointers orientation.

The visualization of the surgical tools on the image data is shown in Fig. 4. The image data is preoperative data. When a resection is performed or when patient anatomy changes due to surgical intervention, this will not be reflected in the image data.

To provide up-to-date imaging, recently a mobile CT scanner, Airo, is available for use in the operating room (Mobius Imaging, Ayer, Massachusetts) which is integrated with the Curve system (Fig. 5). The gantry houses several components including an X-Ray tube, 32-slice helical scan detector array, high-voltage generator, air-cooling system and built-in battery pack. It is placed on a suspension controlled drive system which allows the CT scanner to be moved by one person in and out the OR, on battery power. The gantry can be moved over a guiding rail that is integrated into the drive system. A radiolucent surgical table system is integrated on the drive system (TRUMPF TruSystem 7500, Trump Inc., Farmington, Connecticut, USA). When performing a scan, the gantry moves over its guiding rail while the surgical table system remains stationary. The scanner can operated using the detachable module on the side of the gantry.

The most obvious advantage of an intraoperative CT scanner is the ability to image the actual anatomy of the patient during an operation. The use of intraoperative CT is not new. However, previously described intraoperative CT scanners often required dedicated ORs in which the CT scanner was permanently installed. Mobile fan beam CT scanners were available but also had their limitations including limited bore size and limited scan area [36]–[38]. For the Airo CT, any OR could

Figure 5: Brainlab Curve with two touch screen monitors, the infrared camera and the Airo CT scanner with integrated table system. Image obtainted from Brainlab website.

be used, provided that the OR walls provide enough protection for the radiation. It has a large bore size of 107 cm and a small gantry of 30.5 x 38 cm. Its helical design allows a scan volume of 50x100 cm. Intraoperative CT scans are acquired with 1.0 mm slice thickness. The Airo CT scanner is fully integrated with the navigation system. The gantry contains five reflective markers that are tracked by the infrared camera, which allows for fast and easy registration for navigation. The Airo CT scanner is connected to the Curve navigation system (which is connected to the infrared camera) for automatic transmission of the acquired scan data and automatic registration for navigation.

2.2.2 Preoperative planning

As described in section 2.1, preoperative imaging for bone tumors consists of a CT and MRI scan. Before making an operative plan, the different scans are fused (by image registration, discussed later). This allows the surgeon to make a planning based on both the information regarding bone structures from the CT scan and information regarding soft tissue from the MRI scan. For the operative plan, the surgeon is able to make objects semi-automatically and plan resection planes and screw trajectories on the preoperative images. Additionally, the surgeon can perform the surgery ‘virtually’, e.g. performing resections and plan subsequent reconstruction using implants. This is especially useful in surgeries with complex anatomy, for example a tumor resection in the pelvis. The planning with all of its objects, resection planes and screw trajectories is superimposed on the CT and MRI scan and sent to a dedicated server. The navigation system can access this planning in the OR from this dedicated server. During the operation, this planning can be executed, e.g. cutting along the planned resection planes and inserting screws or implants according to the planned trajectories.

2.2.3 Registration for computer navigation

In order to be able to show the position of the surgical tools relative to the patient on the two monitors, the coordinate system of the virtual representation of the patient needs to be aligned with the local coordinate system of the patient on the operation table. The technique used to align these coordinate systems is called registration. It is the task of finding the geometrical relationship that aligns corresponding points in the coordinate systems [39]. In the operation room, the coordinate system of the patient is the 'central' one. The coordinate system of the preoperative CT and/or MRI scan is rotated and translated to be aligned with the patient coordinate system.

Fig. 6 shows the system setup with the involved components:

1. Infrared camera
2. Patient with attached reference array
3. Virtual representation (e.g. CT and/or MRI)
4. Surgical tool markers
5. Airo gantry markers (only for Airo registration for navigation procedure).

The infrared camera monitors the position of the various markers. The camera has its own coordinate system and the locations of the markers are expressed in this coordinate system. The reference array markers attached to the patient serve as a reference for the local patient coordinate system. Therefore, if the patient is moved, the navigation procedure will still be accurate. Also, the infrared camera can be moved through the operation room while the navigation maintains to be accurate, as long as the reference array is in clear sight of the camera. Since the reference array is the reference for the patient coordinate system, it is important that its position relative to the patient is not altered during the registration process and during the navigated procedure. If its position relative to the patient is altered, the registration process has to be performed again.

The BrainLAB surgical tools are calibrated from factory. Their geometry and shape is available in the navigation system. The surgical tools are tracked by the camera using the attached markers. The system translates the location of the markers in 'infrared camera coordinates' to patient coordinates. Because they are calibrated, the geometry of these tools is known and can therefore be visualized on the image data on the monitors. Additionally, the surgeon is able to calibrate instruments in the OR by using an attachable tool reference tree and a calibration tool.

The gantry markers are used for the registration process: translating the intraoperative CT coordinates to patient coordinates. This is explained in the next section.

Conventional registration methods

If not using the Airo scanner for registration, three widely used registration techniques to align the preoperative CT and/or MRI coordinate system with the patient coordinate system are:

- Paired point matching
- Surface matching

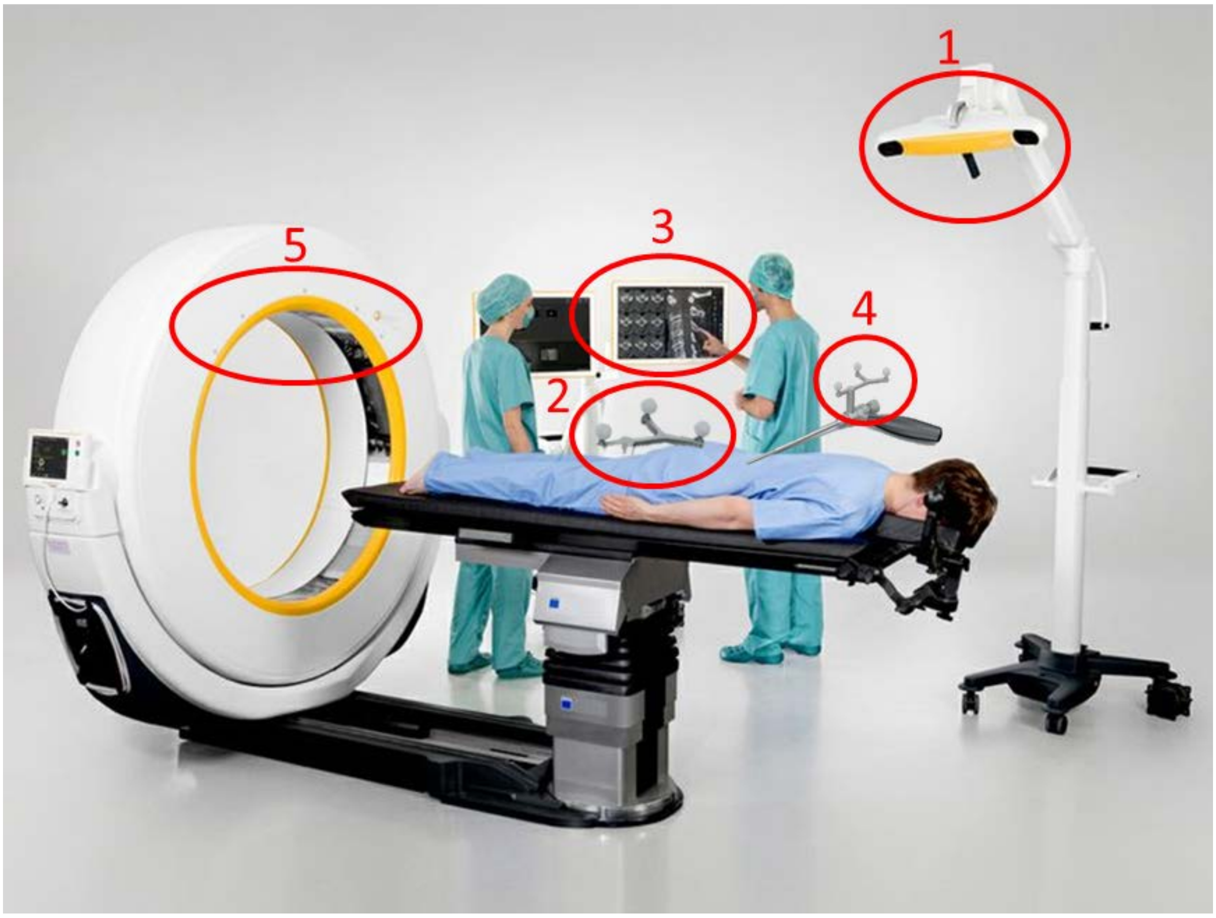

Figure 6: System setup with the involved components for registration for navigation purposes.

- Fluoro-CT matching

The procedure for paired point matching involves defining at least three distinct points in the preoperative imaging. This is usually performed by marking a set of points with the mouse cursor. When performing the registration, the corresponding distinct points on the patient need to be identified using a navigated pointer tool. If both sets of points are defined, the geometrical transformation is calculated using a paired point algorithm. This method requires several user interactions and user input which makes this method error-prone. The quality of the registration depends on the ability of the surgeon to define the exact corresponding points (defined on the preoperative imaging) on the patient using the pointer. To eliminate this step, improvements have been introduced by using markers on the area to be operated on. These markers can easily be identified both on preoperative imaging as intraoperatively using a navigated pointer. This makes exact point-to-point matching easier, resulting in better registration accuracy. The markers can be skin markers or pins, for example. However, this method introduces an extra surgical step – the implementation of the markers which comes with additional risk, patient discomfort and cost [39].

With surface matching, the surgeon moves the navigated pointer along the surface of the patient, in this case bone, thereby creating a cloud of points (surface). These points are mapped onto the surface of the preoperative imaging. The geometrical transformation is calculated when the best fit for the surface has been found using an iterative method [40], [41]. Surface matching obviates the need for preoperatively determined distinct points or preoperatively implemented artificial objects.

Although the intraoperative execution of the two methods is different, their mathematical technique is similar. Both methods use geometrical features (points, lines, surfaces) corresponding to the same anatomical structures to find the geometrical transformation. The only difference is that the paired point method assumes that the correspondences between the points are known while the surface matching method has to iteratively determine these correspondences. In other words, the surface matching method has to 'search' for its corresponding surface in the preoperative image using a similarity function to measure the 'fit'.

Different algorithms are available to find the geometrical transformation for paired points matching, ranging from iterative methods to analytical, direct methods using singular value decomposition, for example. The most frequently used algorithm for surface matching is the iterative closest point algorithm [42]. The algorithms will not be further discussed in this thesis. For further reading about these different algorithms and (image) registration in general, the reader is referred to [43]–[46]. Note that the techniques used for image registration (image fusion) are generally different from the techniques used for registration for navigation purposes.

Fluoro-based matching was introduced as a less invasive method [47]. Generally, fluoro-based matching can be divided into two main categories: feature-based methods and intensity-based methods [39]. Feature-based registration requires segmentation from the fluoro image, a process that is difficult to achieve automatically. Additionally, segmentation errors can lead to registration errors. Intensity-based matching compares the calibrated fluoro images with a digitally reconstructed radiograph (DRR). The DRR is reconstructed from the preoperative CT volume by simulating X-ray projections [48]. The main challenge in this method lies in the similarity measure, which measures the quality of the alignment. The intensity-based method requires more computation time due to the DRR computation, but results in a more accurate registration [39]. Over the years, other methods have been proposed for fluoro-CT matching and the subject is still actively researched [49]–[51].

Intraoperative CT registration method

The introduction of intraoperative CT facilitated a new registration technique. Reflective markers are placed on the gantry of the CT scanner. The CT scanner can be considered a calibrated instrument for which the spatial relationship between the geometry of the gantry markers and the scanned volume is known. When the gantry is in start position to perform a CT scan, the infrared camera tracks the position of the gantry markers and the reference array on the patient. Since the CT scanner is calibrated and the patient coordinate system is defined by the reference array, the rotation and translation matrix can be calculated. When the CT scan is acquired subsequently, the local coordinate system of the scan is rotated and translated using that matrix in order to align it with the patient coordinate system. This method allows for quick and accurate registration and no selection of distinct points, no invasive preparation and no segmentation is required [36], [37]. Not only does it allow for quick registration, the actual anatomical situation can be accurately assessed in the OR instead of relying on preoperative imaging.

Four registration methods for navigation purposes have now been described:

- Paired point matching
- Surface matching
- Fluoro-CT matching
- Intraoperative CT

Paired point matching, surface matching and fluoro-CT matching all use the preoperative CT and/or MRI scan, directly registering the coordinate systems of these scans with the patient coordinate system. Since the planning (if one is made) is attached to this preoperative data, the navigated surgical procedure can be started after registration. When the intraoperative CT is used for registration, the coordinate systems of the preoperative CT and/or MRI scans are not yet aligned with the patient coordinate system. The intraoperatively acquired CT scan is aligned with the patient coordinate system. Performing image registration to align the preoperative CT and/or MRI scans with the intraoperatively acquired CT scan will thus align the preoperative CT and/or MRI scans with the patient coordinate system. To perform this, an image registration workflow has been integrated in the navigation software. The user has to select a region of interest for the volume that needs to be registered and then roughly align the two scans. The navigation software will then calculate the exact alignment of the images. Image registration is only needed if the surgeon decides to use preoperative imaging (with planning, e.g.). Otherwise, the surgeon can perform the navigated procedure using the intraoperatively acquired CT scan.

2.3 Image registration

In order to analyze and compare different images, the images need to be spatially aligned. This process is called image registration and it is frequently used in medical image processing. It is the task of finding the spatial one-to-one mapping from the voxels in one image to voxels in the other image. At LKEB, Elastix is mainly used for image registration, a toolbox for rigid and nonrigid registrations of images. Therefore, the descriptions given in this section are related to image registration with Elastix and are mainly based on the Elastix manual[1] and the corresponding published literature [52]. Since image registration plays a significant role in this thesis, this section contains an introduction to image registration with descriptions of the involved mathematical representations and methods. For more extensive reading on image registration, the reader is referred to [43]–[46].

Two images are involved in the registration process: the fixed image $\boldsymbol{I}_F(\boldsymbol{x})$ and the moving image $\boldsymbol{I}_M(\boldsymbol{x})$. Each image is defined on its own spatial domain. The goal is to find the transformation that makes $\boldsymbol{I}_M(\boldsymbol{x})$ spatially aligned to $\boldsymbol{I}_F(\boldsymbol{x})$. The transformation is defined as a mapping from the fixed image to the moving image. In order to obtain the best possible alignment of two images, the problem is mathematically described as follows:

$$\widehat{\boldsymbol{T}}_{\boldsymbol{\mu}} = \arg\min_{\boldsymbol{T}} C(\boldsymbol{T}; \boldsymbol{I}_F, \boldsymbol{I}_M) \tag{3.1}$$

in which $\boldsymbol{T}$ is the transformation, $\boldsymbol{\mu}$ the parameterization and C the cost function. As can be deduced from the equation, a parameterized transformation is used. An overview of nonparametric methods can be found in [53]. The parameterization contains the available transformations. In other words, the number of possible transformations (e.g. translation, rotation, scaling, shearing) is limited by the parameterization.

The goal is to find a transformation using the parameterization $\boldsymbol{\mu}$ that yields the minimum value for the cost function C. Equation 3.1 can therefore be rewritten as follows:

$$\widehat{\boldsymbol{\mu}} = \arg\min_{\boldsymbol{\mu}} C(\boldsymbol{\mu}; \boldsymbol{I}_F, \boldsymbol{I}_M) \tag{3.2}$$

The cost function consists of two parts, and is defined as follows:

$$C(\boldsymbol{T}; \boldsymbol{I}_F, \boldsymbol{I}_M) = -S(\boldsymbol{T}; \boldsymbol{I}_F, \boldsymbol{I}_M) + \gamma P(\boldsymbol{T}) \tag{3.3}$$

In which S is the similarity measure, P the penalty term or regularization and γ the ratio between similarity and regularity. Several regularization types are available and its function is to constrain $\boldsymbol{T}$ in case of non-rigid registrations. For further reading the reader is referred to the Elastix manual and [54]. For the similarity measure, different metrics are available, which are described in section 2.3.1.

2.3.1 Metrics

Different metrics are supported by Elastix, of which the following are feasible in this thesis:

[1] Available at: http://elastix.isi.uu.nl/doxygen/index.html

- Sum of squared differences (SSD)
- Normalized correlation coefficient (NCC)
- Mutual information (MI)
- Normalized mutual information (NMI)

For the mathematical representation of these metrics the reader is referred to the Elastix manual. SSD compares the intensity for each voxel to voxel mapping and is therefore only suited for images with equal intensity distribution, such as images of the same modality. NCC also uses the intensity values for each voxel to voxel mapping, but assumes a linear relation between the two. It is therefore less strict and can be used more often. MI assumes a relation between the probability distribution of the intensities between the two images. This makes this metric suited for both mono-modal and multi-modal applications (e.g. registration of a CT and MRI image). Normalized mutual information is, just like MI, suited for multi-modal applications.

2.3.2 Sampler

To evaluate the quality of the registration, the metrics described in section 2.3.1 are used. Until now, in the formula's, $\boldsymbol{x}$ represented the voxels in the image. However, it might not be necessary to include all the voxels of the image in the calculation of the metrics. The evaluation of only a part of the voxels in the image might be sufficient and will decrease the calculation time. Several methods are available in Elastix.

Full

All voxels will be selected.

Grid

The sampler places a grid over the image and selects the coordinates of the grid as the voxels used for the metric. This is basically downsampling. The user can select the size of the grid, which is basically a downsampling factor.

Random

Random voxels will be selected. The number of voxels that will be selected can be specified.

Random coordinate

The same as random, but now non-voxel locations can also be selected (e.g. between two voxels). The grey value for the non-voxel location will be calculated by interpolation.

2.3.3 Interpolator

To solve equation 3.1, the location of the moving image with respect to the fixed image is evaluated at different locations. This can lead to evaluation at non-voxel positions (between voxels). In order to obtain grey values for the non-voxel locations, different interpolators can be used.

Closest neighbor

The pixel value of the closest neighbor voxel will be used.

Linear interpolation
The grey value for the non-voxel location is calculated using the average of the surrounding voxels. The weight of each surrounding voxel values is inversely proportional to the voxel distance.

N-th order B-spline
The higher the order, the better the quality, but the longer the computation time. Closest neighbor and linear interpolation are also of this category, with N=0 and N=1, respectively.

2.3.4 Transformations

Several transformations can be used in order to spatially align the two images. The transformations that can be used to align the images can be defined by the user.

Rigid transformation
A rigid transformation allows rotation and translation to align the two involved images. A rigid transformation is defined as:

$$\boldsymbol{T}_{\boldsymbol{\mu}}(\boldsymbol{x}) = R(\boldsymbol{x} - \boldsymbol{c}) + \boldsymbol{t} + \boldsymbol{c} \tag{3.4}$$

With R the rotation matrix, $\boldsymbol{t}$ the translation vector and $\boldsymbol{c}$ the center of rotation.

The parametrization $\boldsymbol{\mu}$ consists of the elements of the rotation matrix and the translation vector. In the case of a 3D registration, the parametrization $\boldsymbol{\mu}$ consists of 6 parameters and is thus defined as:

$$\boldsymbol{\mu} = [\theta_x, \theta_y, \theta_z, t_x, t_y, t_z]^T \tag{3.5}$$

Affine transformation
An affine transformation allows rotation, translation, scaling and shearing of the image. An affine transformation is defined as:

$$\boldsymbol{T}_{\boldsymbol{\mu}}(\boldsymbol{x}) = \boldsymbol{A}(\boldsymbol{x} - \boldsymbol{c}) + \boldsymbol{t} + \boldsymbol{c} \tag{3.6}$$

With $\boldsymbol{A}$ a matrix. The parameterization consists of the elements of matrix $\boldsymbol{A}$ and the translation vector. In the case of a 3D registration, the parametrization $\boldsymbol{\mu}$ consists of 12 parameters and is thus defined as:

$$\boldsymbol{\mu} = [a_{11}, a_{12}, a_{13}, a_{21} a_{22}, a_{23}, a_{31}, a_{32}, a_{33}, t_x, t_y, t_z]^T \tag{3.7}$$

Non-rigid transformation

Non-rigid transformation allows for deformation of the image to fit the other image. This is for example useful when using atlas segmentation. Using non-rigid transformations, the atlas image (or multiple atlas images) can be deformed in order to fit the image of the patient. A commonly used non-rigid registration method is the B-spline non-rigid registration. It uses a uniform grid of control points, which is 'put on' the image, either 2D or 3D (Fig. 7). The control points are moved around in order to deform the image. The spacing between the control points determines the density of the grid, which determines the locality of the transformations. Large grid spacing results in alignment (by deformation) of larger structures while small grid spacing will result in refinement of the deformation of the smaller structures in the image. Ideally, the non-rigid registration is performed using gradually decreasing grid spacing for every resolution (multi-grid). For initial alignment, a non-rigid registration has to be preceded by a rigid or affine registration.

The parameters of $\boldsymbol{\mu}$ are formed by the control point displacements. The number of control points thus determines the number of parameters of $\boldsymbol{\mu}$. The number of control points depends on the image size and the grid spacing.

For an extensive description on the involved parameters in B-spline non-rigid registration, the reader is referred to the Elastix manual.

In Fig. 7 the described transformations are visualized.

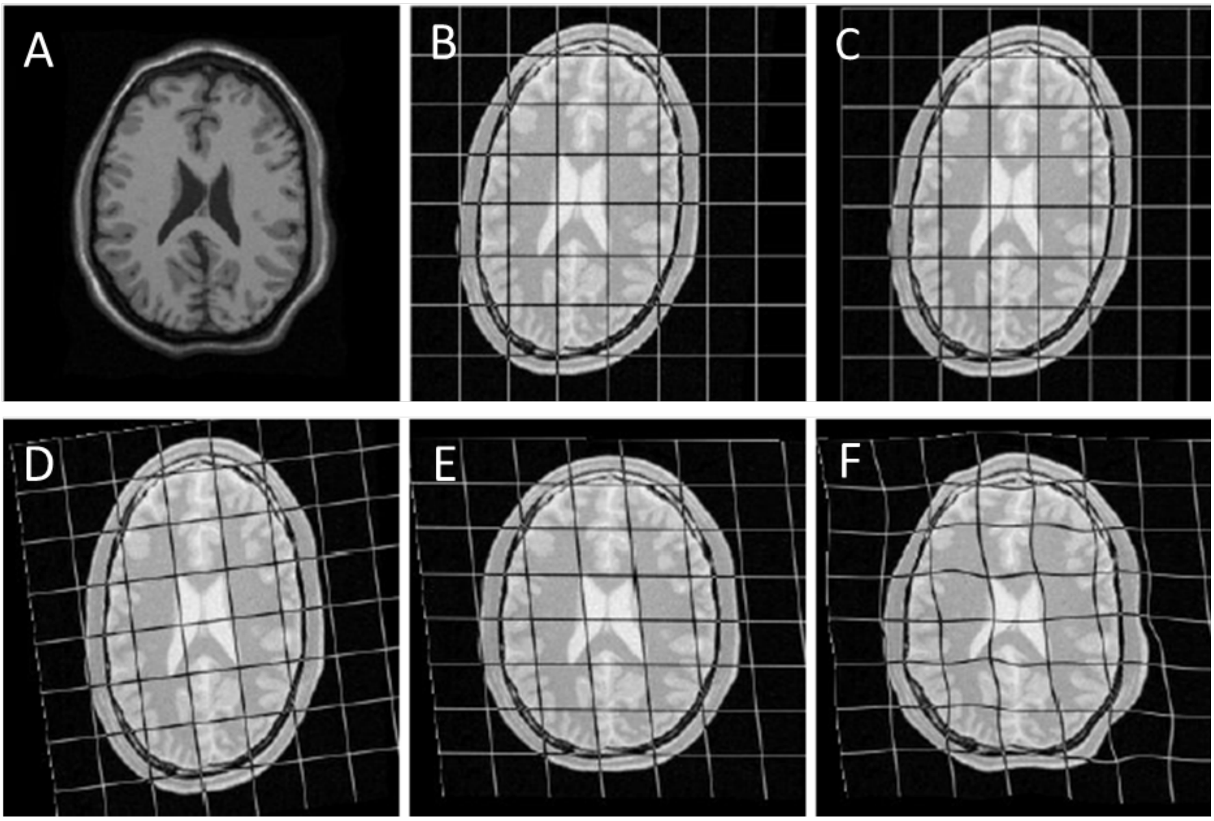

Figure 7: Different transformations visualized with an overlayed grid for clarification. (A) fixed image, (B) moving image, (C) only translation, (D) rigid transformation, (E) affine transformation and (F) B-spline non-rigid transformation. Images obtained from the Elastix manual.

2.3.5 Optimizer

To solve equation 3.1, an iterative method is used, which can be defined as follows:

$$\boldsymbol{\mu}_{\boldsymbol{k+1}} = \boldsymbol{\mu}_k + \boldsymbol{a}_k \boldsymbol{d}_k, \; k = 0, 1, 2, \ldots, \tag{3.8}$$

With $\boldsymbol{d}_k$ the 'search direction' and $\boldsymbol{a}_k$ the step size. This iterative method 'looks for' the values of $\boldsymbol{\mu}$ that yield the lowest cost function. The number of iterations k is user-defined. Different optimization routines can be used, but these will not be described in this thesis. For an overview of different optimization routines the reader is referred to Klein *et al.* [55]. The optimization method that will be used in this thesis is the one that is suggested as default in Klein *et al.*: the adaptive stochastic gradient descent [52], [56].

2.3.6 Multi-resolution

Elastix uses a multi-resolution strategy. This means that early in the registration process images with lower complexity are used, which enhances the chance of a successful registration. This can be accomplished by smoothing and/or downsampling the images. A series of images with increasing amount of smoothing is called a scale space. Smoothing of the images lowers complexity of the images, while down sampling also lowers the amount of data.

Elastix provides three different multi-resolution strategies:

- Gaussian pyramid: applies smoothing and down sampling
- Gaussian scale space: applies smoothing, no down sampling
- Shrinking pyramid: no smoothing, only down sampling.

What method to use also depends on the sampler that is being used. When using a full sampler, and thus selecting all the pixels in the image for the similarity measure, it can be useful to downsample the image early in the registration process to speed up the process. When using the random sampler, this is not necessary, since it will always select the same number of (user-specified) voxels.

In summary, the most important parameters that need to be defined for each rigid or affine registration are:

- Transformation
- Metric
- Sampling strategy
- Interpolation method
- Optimization method
- Multi-resolution strategy

The settings of these parameters depend on the involved images that need to be registered.

3 Joint-preserving excision of an osteosarcoma of the distal femur using intraoperative navigation and intraoperative CT: a case report

R.P.J. van den Ende[1,2], P.D.S. Dijkstra[3*]

[1]Leiden University Medical Center, Department of Radiology, Division of Image Processing, Leiden, the Netherlands

[2]University of Twente, MIRA institute for Biomedical Technology and Technical Medicine, Enschede, the Netherlands

[3]Leiden University Medical Center, Department of Orthopaedic Surgery, Leiden, The Netherlands

Abstract

Navigation guidance in orthopaedic oncology surgery is reported to aid in establishing more accurate margins and increased osteotomy accuracy. Recently, a mobile intraoperative CT scanner was integrated with the navigation system. Its main advantages are automatic registration for navigation and the ability to image the patient intraoperatively. We report on a successfully performed joint-preserving hemicortical resection of a high-grade osteosarcoma of the epiphyseal distal femur using intraoperative navigation and intraoperative CT with subsequent allograft reconstruction.

3.1 Case report

In the past two decades, numerous navigation systems have been introduced to obtain accurate planning and surgery in several disciplines, including neurosurgery, ENT surgery and orthopaedic surgery. Intraoperative navigation can aid in establishing more accurate margins and increased osteotomy accuracy in orthopaedic oncology surgery [1]–[8]. Cartieux *et al.* report significantly increased cutting accuracy in a phantom study with 23 operators each performing four freehand cuts (average 11.2 mm accuracy) and four navigated cuts (average 2.8 mm accuracy) [8]. Additionally, intraoperative navigation can be used for allograft reconstruction, which, in combination with the improved osteotomy accuracy, is reported to aid in improved allograft fit [5], [13], [14]. In our institution, a commercially available navigation system is used (Curve; BrainLAB, Feldkirchen, Germany), in which recently a mobile CT scanner (Airo; Mobius Imaging, Ayer, Massachusetts) was integrated for use in the OR. To our knowledge, no literature is yet available describing the intraoperative use of this specific CT scanner in resection and reconstruction in orthopaedic oncology. This report describes our first experience with the intraoperative CT scanner in an orthopaedic oncology surgery of the distal femur; a patient with a high grade conventional osteosarcoma of the lateral distal femur, treated with en-bloc resection using navigation and intraoperative CT with subsequent allograft reconstruction.

A 19-year-old, otherwise healthy man presented with increasing pain of the lateral right knee for three months. Palpation of the lateral right knee was painful and the anterolateral part of the knee was swollen. Conventional radiographs demonstrated a relatively well-defined expansile osteolytic bone lesion. Magnetic resonance imaging (MRI) demonstrated a heterogeneous T1 iso- to hyperintense and T2 hyperintense eccentric bone lesion of the metaphysis, dimensions 6 × 3 × 4 cm, with profound periosteal reaction and invasion into the soft tissue, suspected for

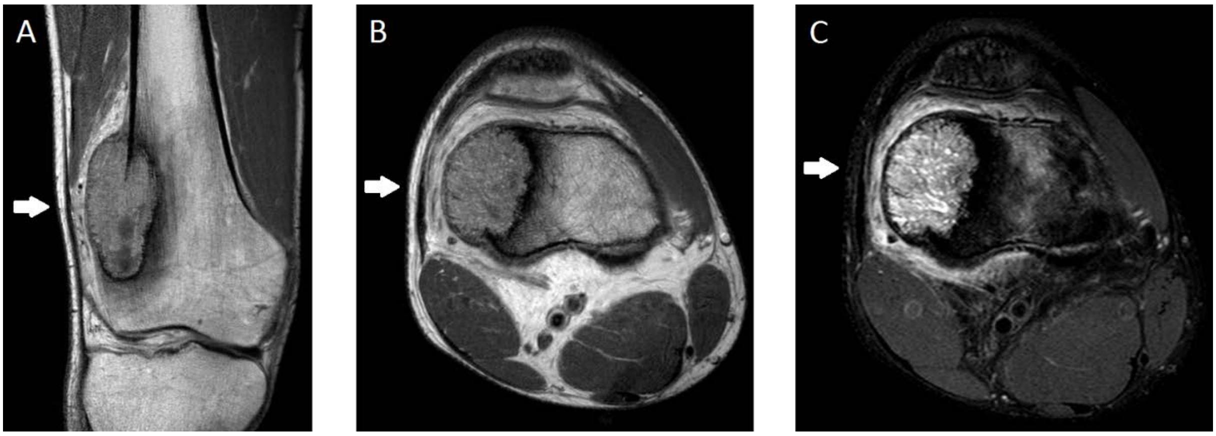

Figure 8: (A) Coronal and (B) axial slices of the T1 weighted MRI. (C) Axial slice of the T2 weighted MRI.

osteosarcoma (Fig. 8). Preoperative CT-guided core needle biopsy confirmed a high grade conventional osteosarcoma. Staging included a thorax CT scan and bone scintigraphy, which demonstrated no other suspected lesions. Treatment plan consisted of neoadjuvant chemotherapy, surgical resection and adjuvant chemotherapy according to the European and American Osteosarcoma Study Group (EURAMOS). After discussing the surgical options, risks, benefits and alternatives at a multidisciplinary meeting and with the patient, a joint-preserving excision of the osteosarcoma followed by allograft reconstruction was chosen.

Preoperative preparation included a CT (1.0 mm slice thickness) and MRI (5.0mm slice thickness, 1.5T) scan. Using iPlan (BrainLAB, Feldkirchen, Germany), the CT and MRI scans were fused, the tumor was segmented semi-automatically and the area to be resected was

Figure 9: Setup of the operating room during surgery.

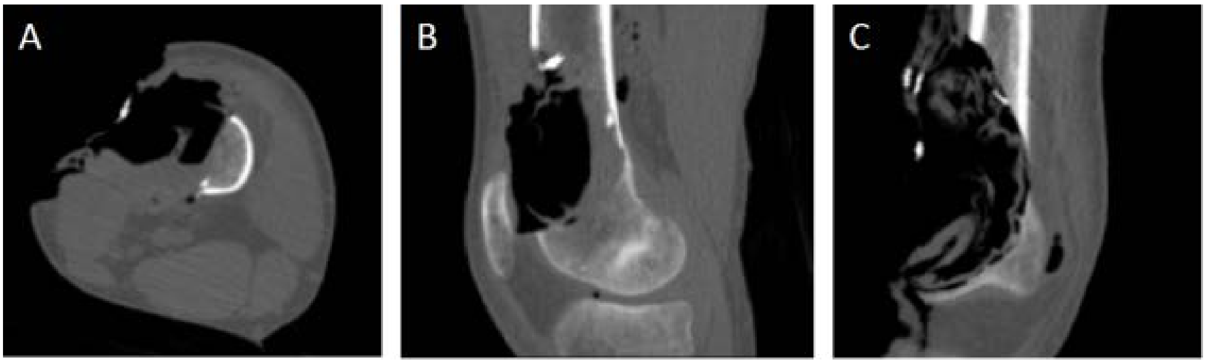

Figure 10: (A) axial, (B) sagittal and (C) coronal slice of the bone defect, as acquired by the intraoperative CT.

planned. The image data and planning were uploaded to a dedicated server and then transferred to the computer workstation in the operation room. The operating room setup is shown in Fig. 9. The intraoperative CT scanner has a large bore size of 107cm, a slim gantry of 30.5 x 38cm, and an integrated surgical table system (TruSystem 7500; Trumpf Medical, Ditzingen, Germany). The CT scanner can be operated using the detachable module on the side of the scanner (Fig. 9). When a scan is performed, the gantry moves on its guiding rail to the appropriate location while the patient table remains stationary. The navigation system consists of a computer workstation with two touch screen monitors, which show the image data and surgical tools and allow user interaction. An infrared camera monitors the position of the patient and the instrumentation. To accomplish this, tracking bodies with small reflective spheres are attached to the patient and the instrumentation. The camera emits infrared light which is reflected by the spheres and the position and orientation of the tracking body is measured. Additionally, reflective markers are integrated in the gantry of the CT scanner for registration purposes. During the scan procedure for registration, the infrared camera tracks the position of both the markers on the reference array attached to the patient and the markers on the gantry, which allows for automatic registration for navigation.

The patient was placed feet first towards the CT scanner in supine position. After lateral approach of the distal femur, two threaded pins were inserted into the cortex on approximately two-third of the femur, on which the tracking body with the reflective spheres was attached. The CT scan was performed, reconstructed and automatically sent from the scanner to the computer workstation. Registration was performed automatically and correct registration was verified using a navigated pointer. Subsequently, the intraoperative image was fused with the preoperative imaging containing the planning in order to use the planning during navigated surgery. The navigated resection of the tumor was performed by using the navigated pointer and an oscillating saw. The cortex was cut around the preoperatively planned resection area. Subsequently, a navigated chisel was used to further excise the tumor. A CT scan was acquired for assessment of resection margins (Fig. 10). Macroscopic evaluation of the resected specimen was performed by a pathologist. After approval that the resection margins were without macroscopic tumor involvement, allograft reconstruction was started. For this, a fresh, frozen cadaver femur (BISLIFE, Leiden, Netherlands) was used, which was reconstructed using an oscillating saw to match the created bone defect. When allograft geometry and proper inlay position was verified with a mobile C-arm with a flat-panel detector (Ziehm Vision FD Vario 3D; Ziehm Imaging, Nuernberg, Germany), a titanium femoral

Figure 11: Resected specimen, minimal tumor margin was 1.4 cm.

locking plate osteosynthesis (Litos Gmbh, Ahrensburg, Germany) was fixated in order to compress the allograft in the remaining bone. The small osseous gaping was filled with morselized spongiosa of the remaining allograft condyle.

Regarding the time we have spent with intraoperative navigation and intraoperative CT: Reference array placement four minutes; CT scan procedure 24 minutes; registration for navigation three minutes, including verification using the navigated pointer; fusion of preoperative and intraoperative imaging 11 minutes, mainly due to the fact that the shifted patella influenced the accuracy. This was solved by selecting a smaller region of interest, excluding the patella. Resection of the tumor took 1 hour and 59 minutes.

Final pathology demonstrated a high grade conventional osteosarcoma with wide margins (minimal tumor margin was 1.4 cm, Fig. 11).

At 9-month follow-up, full weight bearing is achieved without complaints of pain, an X-ray of the allograft shows partial fusion (Fig. 12).

3.2 Discussion

Osteosarcoma is the most common primary tumor of the bone [24]. It tends to arise predominantly in younger people (10-25 years) and older people (60-75 years), mostly in the metaphyses of the long extremity bones, especially around the knee [18]. The standard treatment for high grade osteosarcoma is en-bloc resection along with neoadjuvant and adjuvant chemotherapy. In daily practice, patients with a high grade bone sarcoma of the distal metaphyseal or epiphyseal femur are treated with complete resection of the distal femur and reconstruction using an endoprosthesis which sacrifices the knee joint [18]. However, endoprostheses are related to relatively high complication rates because of loosening, infection, stem fracture, dislocation and component wear [26], [27]. Preserving the joint is therefore preferred, e.g. by performing a segmental resection. However, reconstruction using a intercalary autograft requires long non-weight bearing periods and can cause donor-site morbidity [28]. For intercalary allografts, high complication rates are reported, including fracture, nonunion and infection [29]. A hemicortical resection preserves cortex continuity and excellent complication rates are reported after inlay allograft reconstruction [30]. Therefore, in this

Figure 12: X-ray at 5 months after surgery.

case, it was chosen to perform a navigation-assisted hemicortical resection with subsequent inlay allograft reconstruction.

When excising the tumor, at least marginal margins need to be maintained, since inadequate margins are related to a significantly higher risk of local recurrence [57]. To achieve adequate margins can be a challenge in the case of metaphyseal or epiphyseal resections due to the morphology. The introduction of intraoperative navigation has allowed for guided osteotomy and guided placement of instrumentation. By fusing preoperative CT and MRI, the surgeon can observe the location and extent of the tumor in the bone and soft tissues and make an operative plan [19]. This plan and intraoperative navigation enables the surgeon to avoid critical structures and ensures that the orientation and depth of the instrumentation is adequate for accurate resection of the tumor. The reported increased accuracy in achieving adequate margins and accurate osteotomies enable the surgeon to perform join-preserving surgery in tumors located in the metaphysis [1]–[8].

The main advantage of the intraoperative CT scanner is the ability to image the patient during the surgical procedure, which provides the actual situation, rather than relying on preoperative imaging. This is of paramount importance when using navigation, where the image data is a key element of orientation. Furthermore, imaging of the bone after the resection is especially useful when using intraoperative navigation for allograft reconstruction. In previously published papers regarding navigated allograft reconstruction, the desired 3D model of the reconstruction was based on preoperative imaging and the preoperative plan [5], [13], [14]. When using intraoperative CT, the patient can be imaged after the tumor is resected, thereby imaging the actual geometry of the bone defect. If segmentation of the bone defect is performed directly after CT acquisition, this segmentation could be used as a planning for navigated allograft reconstruction. This will most likely improve the accuracy of the allograft fit to the host bone and is especially useful if the surgeon had to deviate from the preoperative plan.

Geller *et al.* suggested several optimizations for navigation guided surgery with intraoperative CT, including an easier registration process and the ability to merge preoperative planning with intraoperative progress [58]. The registration process in this case required only several minutes. After performing the CT scan, no additional input of the surgeon was required to complete the registration. Fusion of the CT scan performed in the OR with preoperative data was also performed, but this required the selection of a region of interest. There is currently no feedback concerning the accuracy of this fusion.

A disadvantage of intraoperative CT is that the operative procedure has to be interrupted in order to perform a scan. The staff has to move behind lead glass panels to protect them from radiation during the scan procedure. In this case, two lead-glass panels were placed in the operating room. Performing the CT scan and registration took about 27 minutes, because initially the geometry of the markers on the gantry was not recognized by the navigation system. To solve this, the scan workflow on the computer workstation was restarted. The workflow of the scan and registration is simple and (without system errors) this can be performed in less than 10 minutes. Despite this interruption, the fully automated registration is valuable and is expected to enhance the workflow during surgery, compared to conventional registration methods such as fluoro-matching, surface matching and paired points matching.

In summary, this is the first report of a patient with a high grade osteosarcoma of the distal femur, in whom we successfully retained the knee joint, after navigation-guided surgery accompanied by intraoperative CT with subsequent inlay allograft reconstruction. In addition to accurate resections using intraoperative navigation, the intraoperative CT scanner offers a possible improvement in navigated allograft reconstruction by providing intraoperative imaging of the actual bone defect.

4 Navigated allograft reconstruction using intraoperative CT in orthopaedic oncology surgery – a pilot phantom study

R.P.J. van den Ende[1,2], P.D.S. Dijkstra[3], B.L. Kaptein[4], C.H. Slump[1], B.C. Stoel[2]

[1]MIRA Institute for Biomedical Technology and Technical Medicine, University of Twente, Enschede, The Netherlands

[2]Division of Image Processing, Department of Radiology, Leiden University Medical Center, Leiden, The Netherlands

[3]Department of Orthopaedic Surgery, Leiden University Medical Center, Leiden, The Netherlands

[4]Biomechanics and Imaging Group, Department of Orthopaedics, Leiden University Medical Center, Leiden, The Netherlands

Abstract

Introduction: The use of intraoperative navigation in orthopaedic oncology is suggested to aid in accurate tumor resection and achieving adequate margins. Additionally, navigated allograft reconstruction is suggested to improve allograft fit and contact area. However, in published studies, the tumor resection planning is also used for allograft reconstruction. Deviation from planning in tumor resection will make it invalid for allograft reconstruction. This can be resolved by making a reconstruction planning from an intraoperative CT scan. The purpose of this study was to evaluate whether navigated allograft reconstruction using an intraoperative CT-based reconstruction model is more accurate than freehand allograft reconstruction (without navigation), thus leading to a better fit.

Methods: In two femur Sawbones, a hemicortical lateral distal femur resection was performed. For each bone defect, three freehand reconstructions and three navigated reconstructions were performed using femur Sawbones. The reconstruction planning for the navigated reconstructions was made from an intraoperative CT scan of the bone defect. Allograft fit was assessed by determining cortex gap volume between host and allograft.

Results: Mean gap volume for the freehand reconstructions was 3385 mm^3 (range 2355-4422, σ=783) compared to 2191 mm^3 (range 1832-2437, σ=218) for the navigated reconstructions (p=0.01).

Conclusion: In this pilot phantom study, navigated allograft reconstruction using a reconstruction planning made from an intraoperative CT scan of the bone defect led to lower and more consistent cortex gap volumes compared to freehand allograft reconstruction.

4.1 Introduction

Primary bone tumors, especially osteosarcoma, tend to arise predominantly in young people aged 10-25 years [15], [18], [24]. As they mostly arise in close proximity to joints, resection of adjacent joints is often necessitated. Endoprostheses are generally considered the gold standard for joint replacement. However, endoprostheses are related to a relatively high revision rate due to component wear, loosening and infection [26], [27]. Saving the adjacent joint using a segmental or hemicortical resection is therefore favorable. Reconstruction of a segmental resection using a vascularized fibular autograft comes with a substantial risk of fracture until solid union is achieved, which therefore requires long non-weight-bearing recovery. Intercalary allografts have superior initial stability, but suffer from high rates of non-union [29]. A hemicortical resection followed by inlay allograft reconstruction offers several advantages over a segmental resection including preservation of host bone continuity and a larger potential graft-host contact surface. Published studies suggest that an increase in bone contact area between graft and patient bone may improve graft incorporation [5], [14], [32], [59].

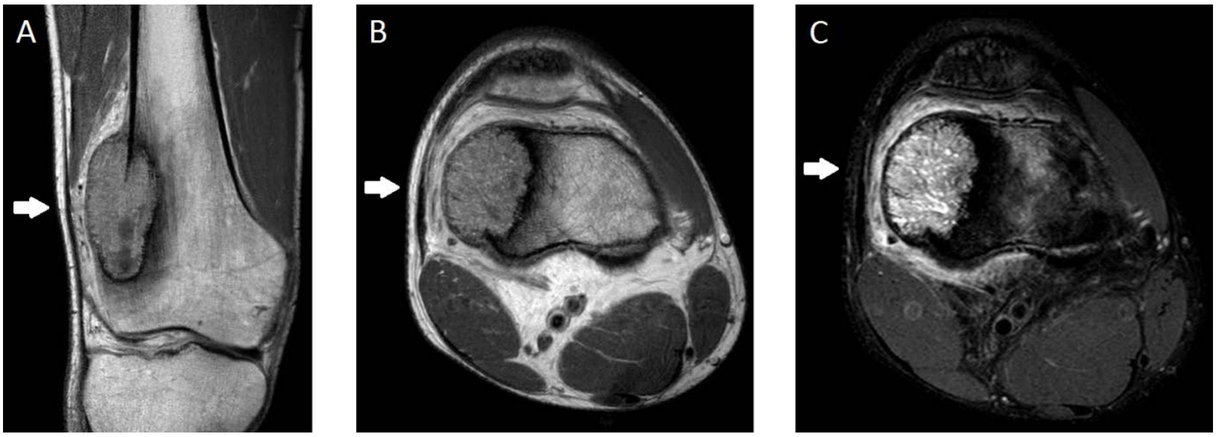

Figure 13: Images of the case on which the experiment is based. (A) Coronal and (B) axial slices of the T1 weighted MRI. (C) Axial slice of the T2 weighted MRI.

The use of intraoperative navigation in orthopaedic oncology surgery is suggested to aid in accurate tumor resection and achieving adequate margins [1]–[8]. The increased osteotomy accuracy may help the surgeon to gain confidence in performing a joint-saving hemicortical resection in epiphyseal bone tumors. Next to that, the navigation system could also be used for allograft reconstruction. Navigated allograft reconstruction is suggested to improve allograft fit and contact area [5], [13], [60]. Published studies used the preoperative resection planning for allograft reconstruction. However, if deviation from preoperative plan was necessary or the resection was not perfectly performed according to plan, the preoperative plan will not be valid for allograft reconstruction. This could however be resolved by using intraoperative imaging. In our institution, a commercially available navigation system is being used (Curve; BrainLAB, Feldkirchen, Germany), in which a mobile CT scanner (Airo; Mobius Imaging, Ayer, Massachusetts) was integrated for use in the OR. This allows imaging of the osseous defect after resection of the tumor. A reconstruction model can be made from the intraoperative imaging, resembling the actual osseous defect, which can be used for navigation-assisted reconstruction of the allograft. Currently, allograft reconstruction is based on measurements using a ruler and the surgeon's visual judgement (so called: freehand allograft reconstruction).

The purpose of this study was to evaluate whether navigated allograft reconstruction using an intraoperative CT-based reconstruction model is more accurate than freehand allograft reconstruction, thus leading to a better fit.

4.2 Materials & methods

Navigation system

The navigation system consists of a computer workstation with two touch screen monitors, which show the image data and the surgical tools. An infrared camera monitors the position of the tracking spheres on the patient and surgical tools. The intraoperative CT scanner is integrated with the navigation system and equipped with tracking spheres on the gantry for automatic registration purposes. The gantry is placed on a battery powered drive system which allows it to be transported to the OR, by one person. It has a large bore size of 107cm, a slim gantry of 30.5 x 38cm, and an integrated radiolucent surgical table system (TruSystem 7500; Trumpf Medical, Ditzingen, Germany). While scanning, the gantry will move over its guiding rail, while the table remains stationary.

Experiment

Foam cortical shell femur Sawbones (Pacific Research Laboratories, Vashon, Washington) were used, which were all identical in shape. The experiment was based on the case of an actual patient who was treated at our department for osteosarcoma of the distal femur (Fig. 13) [61]. On two Sawbones, a tumor resection based on that case was performed, resulting in a bone defect. For each bone defect, three navigated allograft reconstructions and three freehand allograft reconstructions were performed by an experienced orthopaedic surgeon (PDSD). Thus, 2 Sawbones were considered host sawbones (resembling a patient) and 12 Sawbones were considered allografts.

For each reconstruction, the required time was measured. It is defined from the moment the surgeon started marking the osteotomies until the moment a satisfactory reconstruction was achieved. That means that for the navigated reconstruction, this excludes the time needed for scanning the bone defect, making the reconstruction planning, attachment of the reference array to the allograft Sawbone, registration for navigation and image fusion with preoperative imaging with attached reconstruction planning.

Freehand allograft reconstruction

For the freehand allograft reconstruction, the host bone with the bone defect was placed on the patient table. The surgeon was not allowed to perform actions that would not be possible intraoperatively, e.g. picking up the bone. The surgeon marked the reconstruction osteotomies on the allograft bone and performed the reconstruction using an oscillating saw. The reconstruction was refined until a best fit was obtained.

Navigated allograft reconstruction

Fig. 14 contains a diagram with the steps involved in making the reconstruction planning and navigated allograft reconstruction. The following CT scans were involved in making the reconstruction planning and navigated allograft reconstruction (shown in green in Fig. 14):

- Preoperative CT scan: allograft
- Intraoperative CT scan: bone defect
- Intraoperative CT scan for registration for navigation: allograft

After the bone defect was created, an intraoperative CT scan was acquired to image the bone defect (Fig. 14.a). This scan was transferred to iPlan and fused with the preoperative allograft CT scan (Fig. 14.b). The reconstruction planning was made by subtracting the threshold segmentation of the host Sawbone with bone defect from the threshold segmentation of the allograft Sawbone (Fig. 14.c). This results in a segmentation of the bone defect, which was used as a reconstruction planning. Because the scans are fused, the reconstruction planning is attached to both scans. The preoperative allograft CT scan with attached reconstruction planning was then transferred to the Curve (Fig. 14.d). The reconstruction planning was used for all navigated reconstructions of their respective bone defect. That means that Fig 14.a-d was performed once for each bone defect.

To perform the allograft reconstruction, the reference array was attached to the allograft Sawbone on an appropriate location on the area to be used for reconstruction (Fig. 14.e). This will maintain reliable navigation at all times, even after the reconstructed graft is detached from the complete femur. After that, an intraoperative navigated CT scan was performed followed by automatic registration for navigation (Fig. 14.f).

Image registration was performed on the Curve to fuse this scan with the preoperative allograft CT scan with attached planning (Fig. 14.g). Subsequently, the navigated allograft reconstruction was performed according to the reconstruction planning (Fig. 14.h). This was

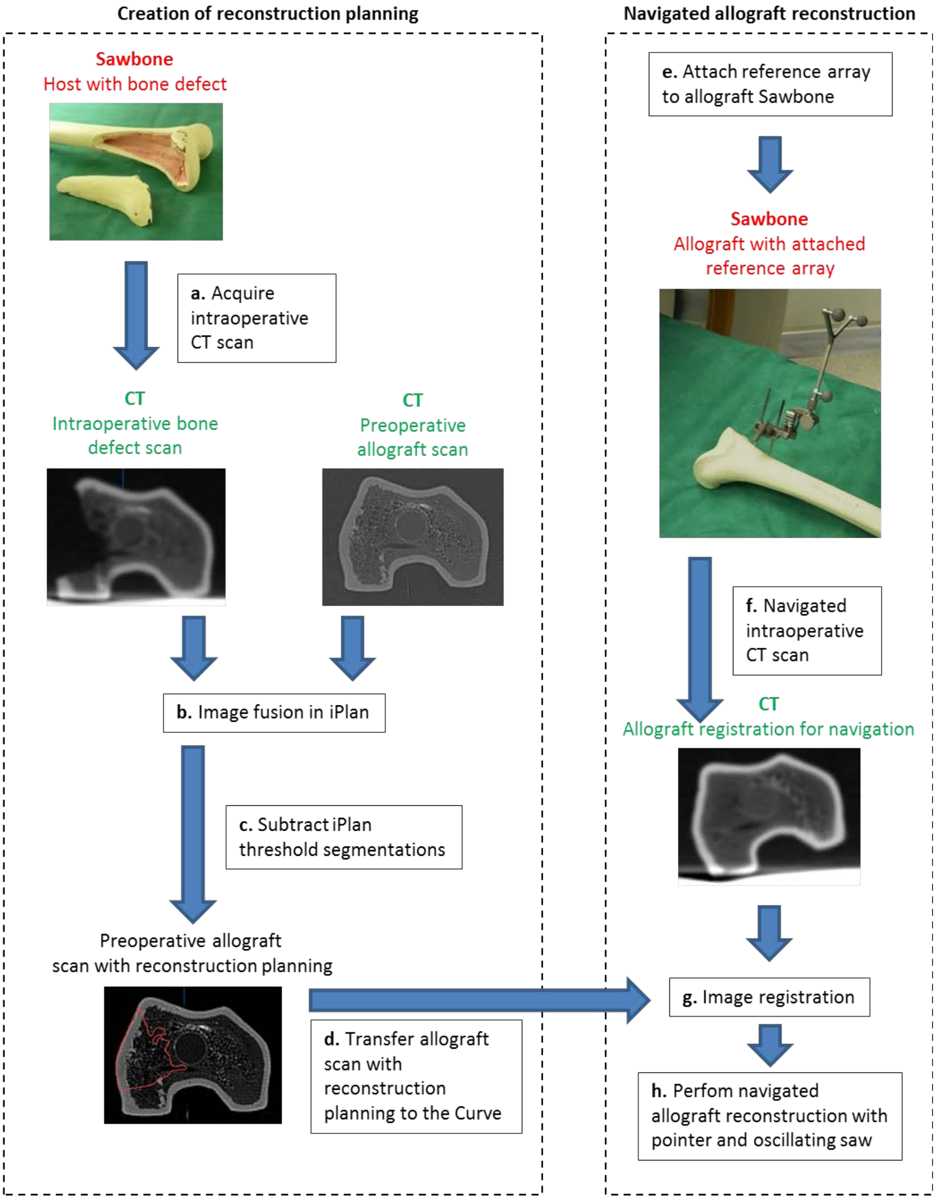

Figure 14: Diagram showing the involved steps to create the reconstruction planning and perform the navigated reconstruction.

achieved by marking osteotomies using a marker and the navigated pointer. The osteotomies were then performed using an oscillating saw. After initial navigated reconstruction, the shape of the allograft was further refined without navigation using the oscillating saw until a best fit was obtained.

Allograft fit analysis

Each reconstructed allograft was fitted and secured in the bone defect and a CT scan of each fitted allograft was acquired for further analysis. Allograft fit was quantified by semi-automatically segmenting the gaps between host and allograft cortices, thereby obtaining a gap volume.

To perform the segmentation, three CT scans were used (shown in green in Fig. 15):

- CT scan of intact host bone (for each host bone)
- CT scan of host bone with bone defect (for each host bone)
- CT scan of host bone with bone defect and fitted allograft

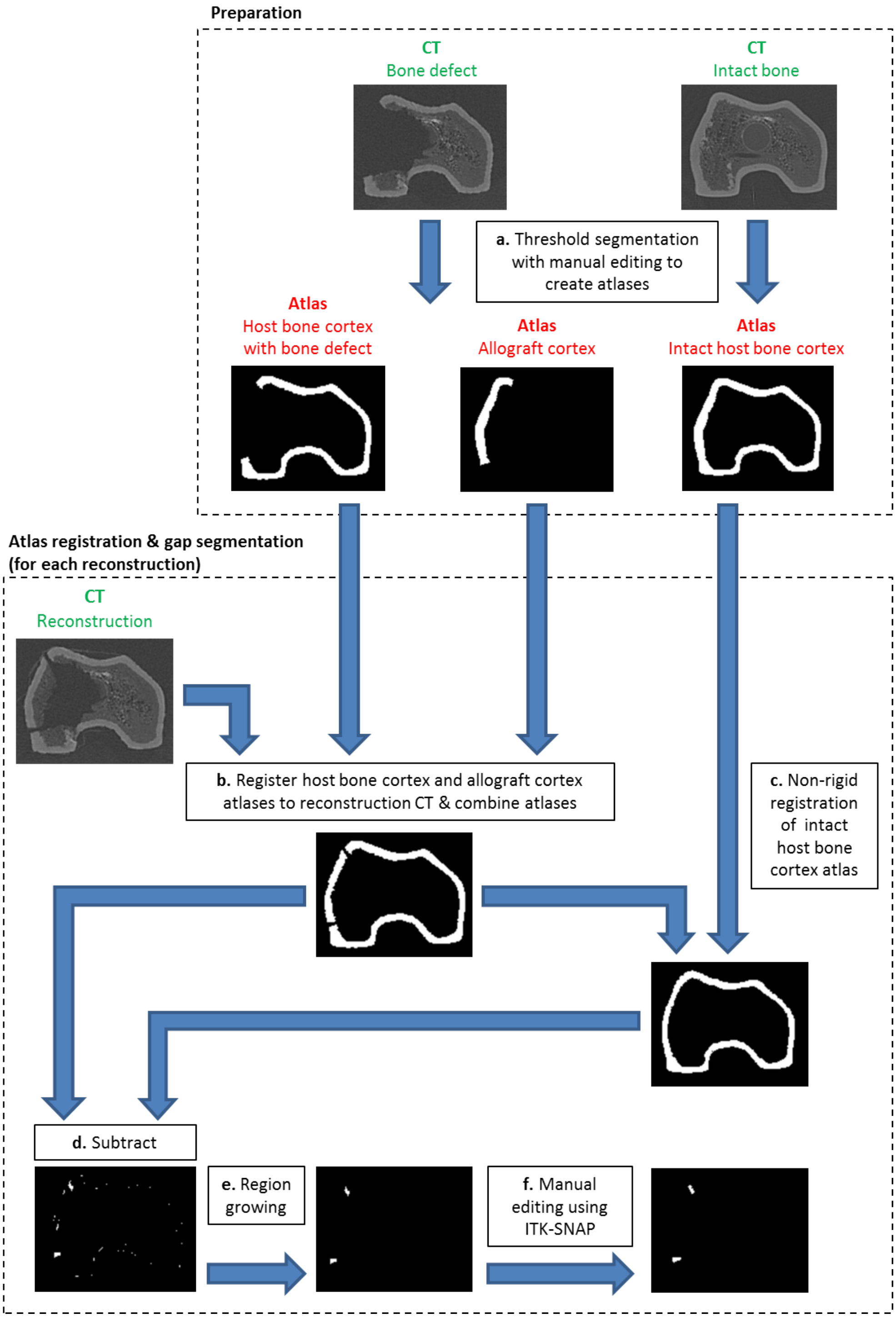

Figure 15: Segmentation steps to semi-automatically segment the volume between host cortex and allograft cortex.

Preparation

Before any gap volumes are segmented, the host bone cortex and allograft cortex need to be segmented. Only applying a threshold did not suffice for cortex segmentation. Therefore, the threshold cortex segmentations were manually edited using ITK-SNAP (Fig. 15.a), a publicly available software program for segmentation of structures in medical images.

The following cortices were segmented semi-automatically and stored as an atlas (shown in red in Fig. 15):

- Intact host bone cortex
- Host bone cortex with bone defect
- Allograft cortex

It is unknown beforehand what the exact dimensions of the allograft will be. The actual allograft reconstruction might be somewhat smaller or somewhat larger than the bone defect due to surgical inaccuracy. Therefore, the allograft cortex atlas is a little larger than the bone defect and it is expected that the actual allograft cortex will fit in this atlas.

Atlas registration and gap segmentation (for each reconstruction)

The created atlases were used to segment the host and allograft cortices on the acquired CT scan of each fitted reconstruction by performing image registration using Elastix [52]. Elastix parameters of the registrations are included in appendix A.

The atlas of the host bone cortex with bone defect was registered in order to segment the host bone cortex (Fig 15.b).

Subsequently, the allograft cortex atlas was registered and the allograft cortex was segmented. (Fig. 15.b; shown in detail in Fig. 16). To accomplish this, the host bone cortex is removed by using the registered host bone cortex atlas (Fig. 16.a). Then, the allograft cortex atlas can be registered to the allograft cortex (Fig. 16.b). The atlas is now registered, but the outer edges of the allograft cortex need to be defined. To do this, the allograft cortex is roughly segmented using a threshold (Fig. 16.c). Subsequently, an AND-operation is performed with the threshold segmentation and the registered allograft cortex atlas (Fig. 16.d). In the resulting image, the largest object is selected to remove segmentation errors (Fig. 16.e). Finally, the registered host bone cortex atlas and the segmented allograft cortex are combined using an OR operation. The gaps are now clearly visible, but need to be segmented.

Gap segmentation is achieved by performing a B-spline non-rigid registration of the intact host bone cortex with the combined segmented host and allograft cortices (Fig. 15.c). Subsequently, the combined allograft and host cortices image is subtracted from the non-rigid registered intact host bone cortex image (Fig. 15.d). Gap volumes can be interrupted when cortices are too close to each other and small segmentation errors are present. To remove segmentation errors and segment the gap volumes, seed points are manually placed in the gap volume at several places for region growing (Fig 15.e). Manual corrections of remaining segmentation errors were performed using ITK-SNAP (Fig. 15.f). To investigate the effect of the manual corrections on the final gap volume, this step was performed twice by one observer.

Statistical analysis

Statistical analysis was performed using SPSS Statistics 21. To compare the fit of the navigated reconstructed allografts with the freehand reconstructed allografts, a Mann-Whitney-Wilcoxon test was used. Intra-user variability in determining the gap volumes was calculated using the intraclass correlation coefficient. The level of statistical significance was set to 0.05 for all statistical analyses.

4.3 Results

Cortex-gap volumes and reconstruction durations are noted in Table 1 and illustrated in Fig. 17. Mean gap volume for the freehand reconstructions was 3385 mm^3 (range 2355-4422, σ=783) compared to 2191 mm^3 (range 1832-2437, σ=218) for the navigated reconstructions (p=0.01). This was 2030 mm^3 compared to 4006 mm^3 for bone defect 1 and 2352 mm^3 compared to 2765 mm^3 for bone

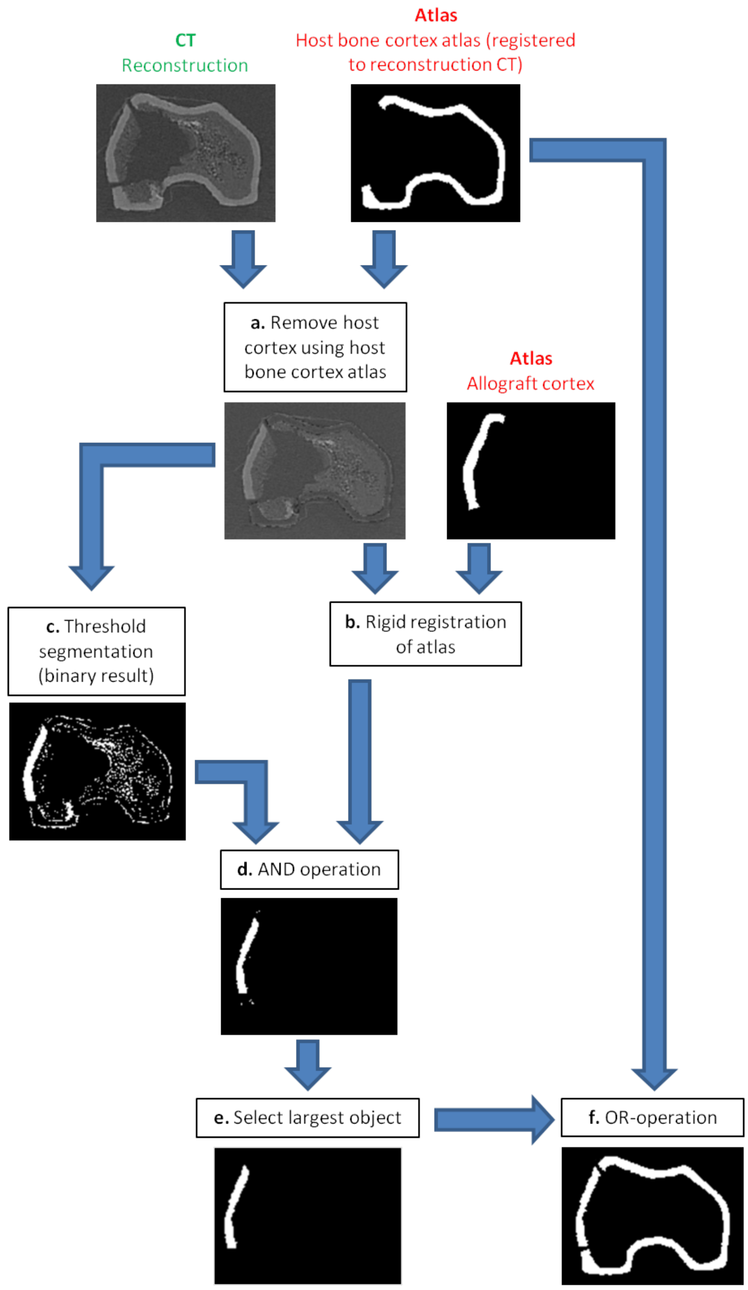

Figure 16: Allograft cortex segmentation

defect 2. These were not significant but it has to be noted that there were only three reconstructions for each method for each bone defect. Mean difference in determining gap volumes was 18 mm^3 (range: -149 – 135, σ = 86). Intraclass correlation coefficient was 0.99.

Mean reconstruction duration was 7.8 minutes for the freehand reconstructions and 18.5 minutes for the navigated reconstructions. Making the reconstruction planning took 40 minutes for bone defect 1 and 30 minutes for bone defect 2. This included the transfer of CT data from the CT scanner to the planning software and from the planning software to the navigation system. Registration for navigation navigated reconstructions was performed in 7-10 minutes, including fusion with preoperative data containing the planning. Attachment of the reference array was performed in 1-2 minutes.

Table 1: Volume of cortex gap and required reconstruction time for each reconstruction

	Freehand reconstruction		Navigated reconstruction	
Bone defect	Cortex gap volume (mm^3)	Reconstruction duration (minutes)	Cortex gap volume (mm^3)	Reconstruction duration (minutes)
1	3743	8	1832	20
	3855	12	2069	18
	4422	7	2189	27
2	2355	6	2437	18
	2626	7	2357	15
	3313	7	2263	13

4.4 Discussion

This phantom study demonstrates the use of intraoperative CT in navigated allograft reconstruction, using the actual geometry of the bone defect, rather than relying on the preoperative planning. The gap volumes produced by the navigated reconstructions were smaller and more consistent compared to the freehand reconstructions. Next to the smaller gap volumes, the navigated reconstructions were easier to fit in the bone defect and it was easier to determine the best fit. The gap volumes for the freehand reconstructions of bone defect 2 were considerably lower compared to bone defect 1. It is unclear what the causes for these differences are. However, some suggestions can be made. First, the number of performed reconstructions is limited, which might contribute to this discrepancy. Second, the freehand reconstructions of the two bone defects were performed on separate days, although no apparent differences in test setup were noted. Third, although both tumor resections were similar, the created bone defects were slightly different. This may have had influence on the difficulty of the reconstruction.

One freehand reconstruction required more time compared to the other freehand reconstructions. During this particular reconstruction it became apparent that there was an error in delivery. That Sawbone was no foam cortical Sawbone but a Sawbone consisting of only cortex-like material. This

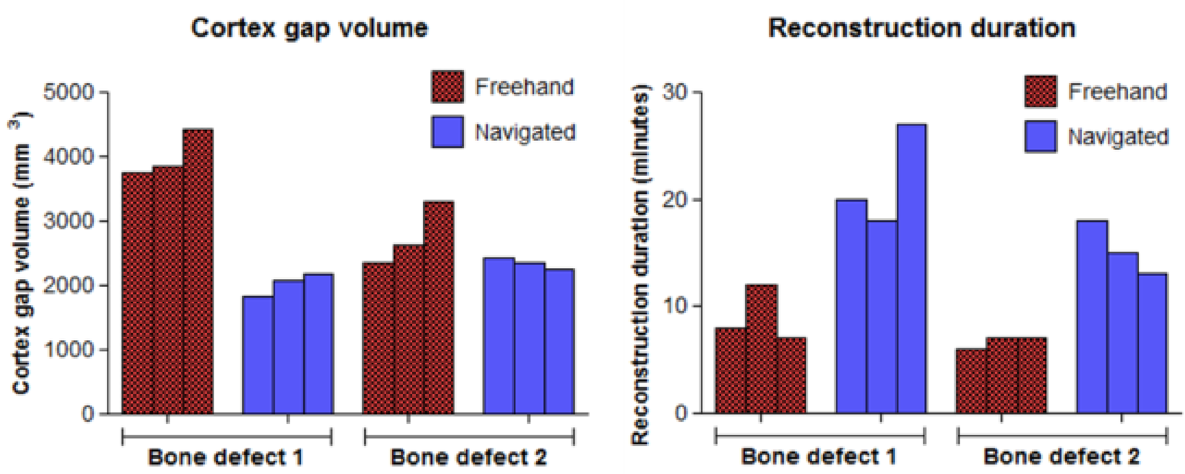

Figure 17: Graph charts showing the gap volume and the reconstruction duration for each reconstruction.

made it more difficult for the surgeon to perform a reconstruction and to detach the graft from the complete Sawbone. Because an alternative Sawbone was not available, it was chosen to include it in the study. We believe the difference in material did not have an influence on the final fit of the reconstructed graft. The navigated reconstructions all required more time compared to the freehand reconstructions. The longer reconstruction times are mainly because the surgeon has to determine the osteotomies using the navigated pointer, which can be time consuming, especially since the reconstruction planning did not only contain straight osteotomies but also curved osteotomies (at the condyles).

Several studies have been published about navigation-assisted reconstruction of allograft bone. Aponte-tinao *et al.* analyzed 69 patients with bone tumors of the extremities who were treated with resection and subsequent allograft reconstruction (47 intercalary, 18 osteoarticular and 4 allograft prosthetic composites). The planning for the reconstruction of the allograft was made before the operation. Although no control group was present in their study, their non-union and infection rates appear to be lower than they previously reported [5], [62], [63]. Docquier *et al.* report a tumor resection in the pelvis with navigated allograft reconstruction. They planned both the resection and the allograft reconstruction before the surgery [13]. Gerbers *et al.* report four patients on which they performed hemicortical resections followed by navigated allograft reconstruction. All allografts were reported to be well-aligned and with good bone contact, except for one allograft [60]. Wu *et al.* mention the use of navigation-guidance for allograft reconstruction using a preoperative plan, but do not report on their experiences [64]. All described studies have in common that the same planning was used for both the resection and the allograft reconstruction. If the planning was not executed perfectly or the surgeon had to deviate from planning, it will not be valid for allograft reconstruction.

Allografts are stored in deep freeze storage. Acquiring a preoperative CT scan of the fresh frozen allograft may include an additional freeze/thaw cycle. This may not present a significant drawback, since recent studies evaluated biomechanical properties after up to eight freeze/thaw cycles and demonstrate little to no effect in fibular allograft bone and bone-patellar tendon-bone allograft [65], [66].

The method used in this study might not represent the actual workflow in clinical practice. In this study, two CT scans are required intraoperatively: one for imaging of the bone defect and one for registration for navigation of the allograft bone. In clinical practice, this would mean that the patient is subjected to two additional CT scans compared to freehand allograft reconstruction. In practice, registration for navigation of the allograft bone should be performed using paired point matching or surface matching. We did not do this in our phantom study, since the paired point matching and surface matching method of the navigation system are designed for spine only and therefore cumbersome to perform on other structures.

Intraoperative creation of the reconstruction planning was performed using iPlan. This was time-consuming and it is expected that it will require even more time in a clinical situation, in which the bones are more difficult to segment and more manual drawing is probably required. Required time may decrease with increased experience, but no data is currently available to support this. Alternatively, methods to automatically segment the bone defect may be developed in order to improve surgical workflow.

Achieving the best reconstruction possible not only involves precise resection and reconstruction, but already begins with the selection of the appropriate allograft. Currently, a 2D template method is used for allograft selection. However, published studies on 3D allograft selection in a virtual environment have reported benefits for pelvis and femur [67]–[70]. It might be beneficial to create a local allograft CT database, as described in Ritacco *et al.* and Wu *et al.* [64], [71]. This could be achieved by routinely acquiring CT scans of the allografts that return from the processing facility before local deep freeze storage. Using a shape matching algorithm, the best allograft can then be selected based on 3D data of the allograft and the patient [64], [67], [71].

Some limitations of our study need to be mentioned.

The reconstructions in this study were performed under ideal conditions. The Sawbones were in full clear view without overlying soft-tissue obstruction. This made it easier to check during a test fit where the allograft needed to be refined in order to achieve the best fit.

All Sawbones were exactly the same shape, which made the reconstructions less complicated compared to clinical practice, especially in determining what area of the allograft to use to fit in the bone defect. It is expected that differences in gap volumes will be larger when graft bones are used with different anatomy compared to the host bone. Additionally, it is also expected that freehand reconstruction duration increases. It will be more difficult to determine what exact part of the allograft will lead to the best fit in the created bone defect. In contrast, it is expected that the navigated reconstruction will not require more time as it still involves the same procedure: drawing osteotomies according to a planning. It is therefore expected that navigated reconstruction will require the same or less time compared to freehand reconstructions in more complex reconstructions.

The number of performed reconstructions was small which makes it difficult to draw conclusions from the observed results. In future (phantom) tests, the number of reconstructions should be higher to increase statistical power and to observe whether the same results will be achieved.

Finally, all reconstructions were performed by one operator. To determine variability between operators and to exclude any bias, multiple operators should be included in future (phantom) tests.

This pilot study is a first step in realizing navigated allograft reconstructions using intraoperative CT. Due to the limitations of this study, a more extensive (phantom) test should be performed to further evaluate the potential and challenges in navigated allograft reconstruction in combination with the intraoperative CT scanner. This test should include host and graft bones with different anatomy, a higher number of reconstructions and multiple operators.

4.5 Conclusion

In this pilot phantom study, navigated allograft reconstruction using a reconstruction planning made from an intraoperative CT scan of the bone defect led to smaller and more consistent cortex gap volumes compared to freehand allograft reconstruction.

5 Evaluation of the clinical use of the Airo CT scanner

To facilitate intraoperative navigation, a computer workstation, the Curve, is available in the OR. Navigated surgery has been used for several years in the LUMC using paired point matching, surface matching or fluoro-matching to register patient anatomy to preoperative imaging. Because the surgeon has to use preoperative images to navigate on, intraoperative anatomical changes will not be reflected. To provide the surgeon with up-to-date information, the Airo CT scanner was integrated with the Curve system for use in the OR. The Curve and the Airo CT scanner are described in section 2.2.1.

The Airo CT scanner was available in the LUMC from October 2014. To date, orthopaedic surgery has performed 16 navigated procedures in 15 patients in combination with the Airo CT scanner. It has been used in nine tumor resections, one tumor biopsy, two deformity corrections (Bechterew and fibrous dysplasia, excluding one revision) and three trauma cases (Table 2). Although the aim of this thesis is orthopaedic oncology surgery, it was chosen to include the trauma cases because spondylodesis (the fixation of multiple spinal levels using screws and rods) is often also performed in tumor cases in the spine.

This chapter is aimed at evaluating the clinical use of the Airo CT scanner in orthopaedic surgery. OR workflow, common problems/errors and their solutions, comparison with conventional methods and (potential) improvements are discussed.

5.1 OR workflow

A workflow diagram of the main preparation for surgery and workflow diagrams of the available registration methods are presented in Appendix C to show the differences in OR workflow between the use of the Airo CT and conventional methods for registration. The descriptions below are guided by the workflow diagrams.

Table 2: Performed Airo procedures from October 2014 to August 2015. iCTs = intraoperative CTs, ED = Effective Dose

Case	Age	Sex	OR date	Pathology	Location	iCTs	ED (mSv)
01	19	M	29-10-2014	Osteosarcoma	right distal femur	2	0,3
02	41	M	4-2-2015	Giant Cell Tumor	S1, S2	3	21,3
03	40	M	9-2-2015	Sarcoma (osteo/chondro)	costa 9 right, T9	2	26,6
04	41	M	26-2-2015	Ewing sarcoma	L1	2	19,7
05	37	M	4-3-2015	Chondrosarcoma	right ilium wing	2	26,5
06	15	M	9-3-2015	Chondroblastoma	left distal femur	1	0,2
07	16	M	18-3-2015	Fibrous dysplasia	left femur	4	1,5
08	60	M	20-4-2015	Bechterew, fracture L3	L3	3	34,5
			28-4-2015	Bechterew, screw revision	L1 L2	4	72,1
09	43	F	20-4-2015	Biopsy unknown tumor	T8	2	13,8
10	59	F	8-6-2015	Chondrosarcoma	T10, T11, T12	2	31,0
11	64	M	3-7-2015	Trauma, fracture	T4, T7, T8	3	30,2
12	54	M	13-7-2015	Ewing sarcoma	O. Naviculare, left	3	0,4
13	55	M	13-7-2015	Trauma, fracture	T4	3	32,6
14	70	F	21-7-2015	Trauma, fracture	T5	4	42,5
15	47	F	3-8-2015	Osteosarcoma	left distal femur	1	0,3

Preparation

The scanner has to be prepared in order to use it in the OR together with the Curve navigation system. Since the CT scanner is not routinely used every day, it first needs to be transported from its storage location to the other side of the OR complex. This generally takes about 5-15 minutes, depending on the experience of the 'driver'. The Airo CT scanner has to be placed in the OR according to the OR setup that is always used in orthopaedic surgery (Appendix B1 and B2). We believe this to be a convenient setup as it divides the OR in two sides: the anesthesiologist and radiographer on one side and the sterile surgical team on the other side. This is convenient when performing a scan procedure, having all sterile personnel behind one lead glass panel and remaining personnel behind the other lead glass panel. Care has to be taken to ensure that the gantry is able to move outside the down flow area when not being used.

Before the scanner can be used, an emergency stop test and a warm-up scan have to be performed. These can be performed directly after the scanner is placed in the OR, connected to the power socket and prepared for scanning (rotating the gantry and homing the tilt). The scanner also shows that a gain calibration has to be performed. Before the gain calibration can be performed, the detectors need to warm up for which a fixed counter of 30 minutes is used. During this time, the patient cannot be transported into the OR, since the patient will then be exposed to the radiation emitted during the gain calibration.

Scan procedure

After attachment of the reference array to the patient bone, a navigated CT scan can be acquired. The workflow for the scan procedure can be started using the Curve (by selecting 'new Airo scan') or the Airo detachable module ('new scan'). When the scan workflow is started, all staff in the OR will take place behind the lead glass panels with exception of the radiographer, the anesthesiologist and the surgeon. The radiographer performs the workflow on the detachable module of the Airo: selecting patient weight, patient orientation and which body part will be scanned. After that, the start- and end-position of the gantry is defined by the radiographer according to the surgeon's instructions, using the laser on the gantry. If chosen to perform a scout scan, the scout scan can now be performed using the selected start and end point (radiographer, surgeon and anesthesiologist position themselves behind lead glass panels). After that, the range of the 3D scan can be selected on the scanogram. Just before the 3D scan is acquired, the markers on the gantry and the markers on the reference array have to be in camera view. The Curve uses the positions of these markers to calculate the registration for navigation. After the anesthesiologist stops patient breathing (if necessary, depending on what part of the patient is scanned), the 3D scan is acquiered. When the scan is completed, patient breathing is continued and the acquired scan is transferred from the Airo to the Curve navigation system, which automatically starts the navigation workflow. In this workflow, preoperative data (with planning) can be fused to the acquired intraoperative CT scan. Subsequently, the surgeon checks for correct navigation with a navigated pointer and the operation procedure can be continued. A non-navigated 3D scan (for screw position verification, for example) is acquired in the same way. In that case, however, the reflective markers on the gantry and the reference array (if still attached) do not have to be in camera view.

Learning curve

The duration of the scan procedure has been substantially reduced since the introduction of the Airo CT scanner. The duration of the 'scan procedure' is defined as the time between the start of the scan

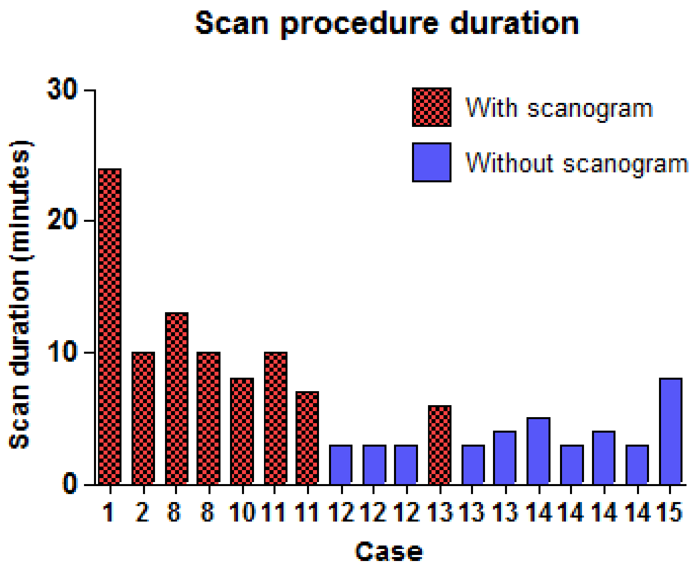

Figure 18: Scan duration times for several operations procedures in several cases.

workflow on the detachable module and the end of 3D scan acquisition. The scan procedure duration was recorded for 18 of 42 performed scans. As shown in Fig. 18, scan duration time is reduced since the introduction of the Airo CT scanner. Average scan time was reduced to about 3-4 minutes, if no system errors were present. The red bars indicate scans with use of a scanogram, the blue bars indicate scans without use of a scanogram.

The shorter scan times are achieved because the scanogram is no longer used and the radiographers become more experienced over time. Skipping the scanogram saves time because the scanogram is not acquired by the scanner, no selection of 3D scan area on the small detachable module is required and a common unknown system error (bug) often arising in the scanogram workflow will not occur. Additionally, the radiographers become more experienced over time and are more confident in performing the workflow on the detachable module and moving the gantry over the guiding rail, while paying attention that enough clearance is available to surrounding objects (anesthesia hardware, wires, hoses).

5.2 Common problems, challenges, errors & solutions

As with any new technique, its introduction in clinical practice may come with several challenges, problems and bugs: both hardware-based and software-based. These challenges, problems and bugs are described in this section, along with an explanation (if known) and solution.

Gain calibration

The Airo CT scanner prompts on every startup that a gain calibration has to be performed. However, this is not necessary as once in a week or two weeks is sufficient. Since both the Department of Radiology and the Department of Orthopeadic Surgery were not aware of this, the scanner was always gain calibrated before every first operation of the day. Especially when the operation procedure for which Airo is used is not the first one in the OR that day, delays were often encountered. It is therefore recommended to perform the gain calibration once a week on a scheduled moment, for example every Monday morning before the first operation procedure.

In the first seven procedures we performed, the gain calibration mostly failed, without reported reason or 'severity' of the failure. When this happens, it is advised to acquire a CT scan of any object to check whether the acquired scan looks normal. When a complete detector row, for example, was broken, this would clearly be noticeable in the acquired CT scan. BrainLAB replaced a detector row and since then, we have not experienced any failures in the gain calibration anymore. Despite the failed gain calibrations in the first seven procedures, the Airo CT scanner was used without image quality problems.

Initiation of the scan workflow

The scan procedure workflow can be started in two ways: on the Curve or on the Airo CT scanner. Both systems need to be aware that a navigated scan will be acquired. However, while already going through the workflow on the Airo, the Curve will not be triggered until halfway through the workflow. If (for some reason) on the Curve 'new Airo scan' is selected, it seems that a mismatch occured: when the scan is performed and sent to the Curve, it will not recognize the CT scan as a navigated CT scan. BrainLAB has confirmed this error after evaluation of the logs and the acquired CT scan. When the Curve does not recognize the navigated CT scan, end the 'current treatment'-procedure on the Curve and start a 'new treatment'-procedure (without patient selection). If the acquired CT scan is now transferred from the Airo to the Curve, the navigation workflow will automatically be started and the scan will be recognized as a navigated scan. We have experienced this problem in 6 of 16 performed procedures.

Visualization of the scanogram

If it is chosen to perform a scanogram before the actual 3D scan, the scanogram cannot be transferred to the Curve in order to view it on one of the monitors. Instead, the surgeon has to view the scanogram on the small detachable unit and determine from that small view what the scan area has to be for the 3D scan that will subsequently be acquired. BrainLAB will include transfer of the scanogram to the Curve in the next update (expected October 2015).

Error in scanogram part of scan workflow

Just before, during, or just after the scanogram step in the scan workflow, an unexpected system error randomly appears and the CT scanner has to be restarted. This is reported to BrainLAB, acknowledged and it will be fixed in the next update (expected October 2015).

Recognition of reflective sphere geometry

In two of sixteen procedures, we encountered a problem with the recognition of the reflective sphere geometry of any object, e.g. the reference array. All reflective spheres are displayed on the Curve system but flicker intermittently and are not recognized as an object. This seems to be caused by reflective spheres that are not clean enough. After cleaning the reflective spheres thoroughly, the problem was solved. This also explains the longer scan duration time in case 15 (Fig. 18).

Separate C-arm needed for placement of implant

When placing an implant (e.g. a cage in the spine), its placement has to be verified. Normally, this is performed using a C-arm. Since a correct cage position is difficult to achieve, several verifications often need to be performed. Acquiring an intraoperative CT scan for each verification would be time consuming and patient radiation dose would become too high. However, there is barely enough room for a C-arm in an OR in which the Curve and the Airo are also positioned. This makes verification using a C-arm a cumbersome procedure. It would be useful if the Airo CT scanner was able to perform the verification by for instance performing a scanogram. However, up till now, this is not implemented in the scanner options. When implemented, the user should be able to select the angle at which the scanogram is acquired and the result should be visualized on the monitors of the Curve system.

5.3 Comparison with conventional registration methods

5.3.1 Registration and preparation

In this section, a comparison of the registration methods is given in terms of required preparation and performing the registration. The descriptions for each of these registration methods are already given in section 3.2.3. As with any described registration method, the registration is performed after attachment of the reference array to the patient.

Paired point matching

Paired point matching requires selection of points on preoperative data after which these points are defined on the patient using a navigated pointer. A minimum of four points has to be selected and in practice minimal eight points are usually used.

For paired point matching, only the Curve and the infrared camera have to be prepared. During the registration procedure, all OR staff can remain at their position. Paired point matching is easier to perform in vertebras, for example, where anatomical landmarks are clearly present. However, in long bones for example, it is more difficult to select the appropriate points on the patient. Although paired points matching requires less preparation, it is expected that in orthopaedic oncology procedures on the femur or pelvis for example, the actual registration will be more time consuming compared to registration using Airo.

Surface matching

Surface matching requires the selection of a surface on preoperative data after which the corresponding surface on the patient is tracked using a navigated pointer.

For surface matching, only the Curve and the infrared camera have to be prepared. During the registration procedure, all OR staff can remain at their position. The downside of this method in the Curve navigation system is the fact that it can only be used for registration of pedicles, for which its effectiveness has been proven. We have tried to use it for registration of the pelvis or femur, but it is not guaranteed to be successful. Especially when using this system for orthopaedic (oncology) surgery, other structures as the femur or pelvis have to be registered. Because the registration of structures other than pedicles is not supported, it is recommended to use fluoro-matching or the Airo for registration for navigation in those structures.

Fluoro matching

With fluoro matching, registration for navigation is performed by acquiring two images, one anterior and one oblique, while the x-spot is placed on the patient.

When using fluoro matching, the Curve, infrared camera and a fluoroscopic device have to be prepared. All OR personnel can remain at their positions but need to be protected against the emitted radiation during image acquisition by wearing lead aprons. Fluoro-matching can provide registration for navigation on any anatomical location. However, it is expected that the registration for navigation using the Airo scanner requires less time.

5.3.2 Radiation exposure

Possible long-term deleterious health risks associated with low-dose radiation exposures remain unclear [72]–[74]. However, it is the surgeon's responsibility to strive for as low as reasonably achievable (ALARA) radiation exposure. To assess radiation exposure in the procedures in this study, the dose length product (DLP) for each scan of each patient was obtained. To calculate the effective dose, the normalized effective dose per DLP conversion factors were used (0.019 for chest, 0.017 for abdomen and pelvis and 0.0008 for legs) [75]. The number of scans and total effective dose for each procedure are noted in Table 2.

A total of 42 scans were performed in 16 procedures on 15 patients. Average numbers of scans was 2.6 (range 1 – 4). In some procedures, more scans were acquired than normally necessary, because of three reasons:

- Loss of navigation accuracy (three extra scans)
  In case 2, 9 and 14 an additional registration for navigation scan had to be performed because of inaccuracy of the navigation. This accounted for an additional effective dose of 7.1, 11.1 and 9.9 mSv, respectively. In case 2, the reason was unknown. In case 7 and 14 it was caused by inadequate fixation of the reference array. In all cases, the additional registration for navigation was successful and remained accurate for the rest of the procedure.

- Metal artifacts (two extra scans)
  In case 8, two additional scans were required. This accounted for an additional effective dose of 27.9 mSv. In the first scan, the image was severely distorted by artifacts. Not knowing what the cause was, another CT scan was acquired, hoping that it would be successful. After the second distorted CT scan, it was discovered that a special cushion containing metal was used to place the patient in proper position. This cushion is normally not used, which is probably why it took two CT scans until this was discovered.

- Software error (two extra scans)
  In case 7, two extra CT scans were acquired. This accounted for an additional effective dose of 0.7 mSv. The first registration scan in case 7 was not recognized as a navigated scan. This error is described in section 5.2. At the time of case 7 we did not know yet how to fix this issue without acquiring an extra CT scan. Therefore, an extra CT scan was acquired. However, the extra CT scan was also not recognized as a navigated scan and the surgeon decided to abort the navigation procedure and continued the operation without navigation.

The calculated patient dose for the performed procedures in our study was compared to other studies. Only studies were found that evaluated radiation exposure in pedicle screw placement in spine surgery. To make a fair comparison, only the spine procedures with screw placements in our study were included (case 2, 4, 8, 10, 11, 13 and 14). Additional scans that were required because of loss of accuracy and metal artifacts were excluded. This results in an average effective dose of 29.9

mSv (range 14.2 – 44.2), an effective dose per single level of 7.3 mSv (range 3.8 – 14.7) and 2.5 (range 2-3) intraoperative CT scans per patient.

Lee *et al.* reported a mean effective dose of 15.8 mSv (range 9.4 – 27.2) using intraoperative CT in 37 patients for transpedicular screw fixation to treat unstable thoracic and lumbar spine fractures [76]. Effective dose per single level was 2.7 mSv and the average number of intraoperative CT scans per patient was 2.1 (range 2 – 3). The number of scans and average effective dose in our study is higher compared to the study of Lee *et al*. The difference might be explained by different scan parameters, which were not mentioned in their study. Additionally, when reviewing the acquired intraoperative CT scans in our study, scan acquisition length was sometimes substantially longer than imaging of the involved vertebras would require. It is unknown why such large scans were acquired. To potentially reduce radiation dose, it should be researched why such large scans were acquired and if this was performed on purpose.

The use of intraoperative CT results in higher radiation doses compared to conventional methods of pedicle screw placement: both the freehand 2D fluoroscopy-guided technique and the navigated technique with fluoro-matching. Bronsard *et al*. reported average effective doses of 0.55 and 1.51 mSv in freehand open screw placement and freehand percutaneous screw placement, respectively [77]. Villard *et al*. report a mean dose area product of 1885 $cGy \cdot cm^2$ for the freehand 2D fluoroscopy-guided technique and 887 $cGy \cdot cm^2$ for the navigated technique [78]. No effective dose calculations were given. Effective dose conversion factors in $mSv/Gy/cm^2$ vary according to the anatomic region the X-ray was acquired: frontal thoracic spine = 0.27, lateral thoracic spine = 0.1, frontal lumbar spine = 0.21, lateral lumbar spine = 0.13 [77]. Using these dose conversion factors, an average effective dose range can be calculated in which the real average effective dose must be. The reported average dose area products of Villard *et al.* would then result in 1.88 – 5.09 mSv for the freehand technique and 0.89 – 2.39 mSv for the navigated technique. No data was present on the effective dose per single level in both studies. The described comparisons are noted in Table 3. Note that for the studies without intraoperative CT, a postoperative CT scan has to be acquired to verify screw positions, adding to the reported effective doses.

Although patient groups, indications and techniques differ between the mentioned studies, above comparisons show the order of magnitude of radiation exposure of conventional methods. The comparisons are only made for the spine procedures in our study (both trauma and tumor cases). It is difficult to compare the remaining tumor procedures to other studies as indications and techniques vary widely.

Table 3: Average effective doses per procedure reported by other studies compared to this study. iCT = intraoperative CT

Study	Freehand with 2D fluoroscopy guidance	Navigation with fluoroscopy	Navigation with iCT
Lee *et al*.	-	-	15.8 mSv
Bronsard *et al*.	0.55 - 1.51 mSv	-	-
Villard *et al*.	1.88 - 5.09 mSv	0.89 - 2.39 mSv	-
This study	-	-	29.9 mSv

Typically, during spine procedures with subsequent screw fixation, two or three CT scans are acquired: one for registration for navigation, one for verification of the K-wires (if used) and one for verification of final screw positions. It has to be noted that the CT for verification of final screw positions would otherwise have been performed postoperatively. That means that only the scan forregistration for navigation and the optional scan for verification of K-wires should be considered added radiation exposure as a consequence of using intraoperative CT in pedicle screw placement.

5.4 Substantial improvement for orthopaedic oncology surgery?

The added value of a navigation system in orthopaedic oncology surgery is well established. Is the introduction of the Airo CT scanner also of added value for orthopaedic oncology surgery? The three main advantages of the Airo CT scanner are:

- Easy automatic registration for navigation
- The ability to visualize current anatomy during surgery
- The ability to acquire image data in 3D instead of 2D

These advantages are useful during certain orthopaedic oncology surgeries and applications.

Easy automatic registration for navigation
Conventional registration methods have been described (paired point matching, surface matching and fluoro matching). The BrainLAB software was designed for brain and spine surgery and orthopeadic surgery is not supported. This makes conventional registration methods sometimes unsuited for registration of pelvis, tibia or femur, for example. With the Airo, registration on any anatomical location can be performed without problems. Next to that, it is easy to perform and after acquiring the navigated intraoperative CT scan, registration for navigation is automatically completed.

The ability to visualize current anatomy during surgery
Allograft reconstruction
Included in this thesis is an article about a pilot phantom study about navigated allograft reconstruction using intraoperative CT. Although the actual clinical application of navigated allograft reconstruction using the intraoperative CT is not yet implemented, it is considered a potential substantial improvement over conventional reconstruction methods mentioned in literature and currently used in the LUMC.

Spine
Using navigation in spine procedures should be performed with caution when using preoperative image data. Preoperative CT scans are often acquired in supine position while the patient on the OR table is positioned in prone position. The anatomical relationships between vertebras differ between the two positions. When using navigation with conventional registration methods, the surgeon has to perform registration for each one or two pedicles in order to maintain reliable navigation. With the Airo CT, the intraoperatively acquired CT scan can be used for navigation, which reflects the exact patient position on the operation table.

Screw placement evaluation
Conventionally, CT imaging of screw positions is performed the day after surgery. However, if any of

the screws is misplaced, the surgeon has two options: accept the misplacement or perform revision. The last option requires extra surgery. When placing screws under navigation guidance using intraoperative CT, depending on the method and location, screw placement is verified twice: once after placement of the K-wires (if used) and once after final screw placement. This is considered a substantial improvement, being able to accurately spot any screw misplacement and revise it directly. This can reduce the need for a second operation for revision of misplaced screws [76].

The ability to acquire image data in 3D instead of 2D

CT imaging is the gold standard for confirmation of screw positions [79]. Especially in the case of pedicle screws, (intraoperative) plain antero-posterior and lateral radiographs or 3D fluoroscopy insufficiently verifies screw positions [76], [79]. Especially in the case of screw placement in complex anatomy like thoracic vertebras or the pelvis, screw positions can be verified more accurately using the Airo CT scanner.

In the case of extensive oedema, for instance after trauma, the use of a C-arm to place screws can be problematic. The image will not be of sufficient quality due to the oedema. Operations might therefore be postponed until oedema is reduced or disappeared. Using the Airo CT scanner, this is not considered a problem and the operation can be performed.

It has to be noted that the image quality produced by the Airo scanner was not evaluated in this thesis. Scan parameters are pre-defined according to selected patient weight and body part to be scanned. The operator can choose from three reconstruction kernels: soft, standard or sharp. No manual editing of scan parameters or reconstruction options was possible.

In summary, the use of the Airo CT is considered a substantial improvement for orthopaedic oncology surgery. The main advantages of easy automatic registration for navigation, visualizing the current anatomical situation and superior 3D image quality are beneficial in tumor resection, allograft reconstruction and screw placement in spine, pelvis and extremities. However, this comes with the disadvantage of higher patient radiation dose.

6 Conclusion

The two research questions formulated in the introduction of this thesis were:

1. Does navigated allograft reconstruction using a reconstruction planning from intraoperative CT lead to more accurate allograft reconstructions compared to freehand allograft reconstruction?
2. Is the new intraoperative CT scanner a substantial improvement for orthopaedic oncology surgery, a discipline for which it was not specifically designed?

1.

According to the results in the pilot phantom study, navigated allograft reconstruction using a reconstruction planning made from an intraoperative CT scan leads to lower and more consistent cortex gap volumes, thus leading to a better allograft fit, compared to freehand allograft reconstruction. The use of an intraoperative CT scanner enables the surgeon to reconstruct the allograft based on intraoperative imaging of the bone defect. This is considered an advantage over the navigated methods used in other studies.

However, as it was a pilot study, the number of reconstructions was limited. A more extensive (phantom) test should be performed to further evaluate the potential and challenges in navigated allograft reconstruction in combination with the intraoperative CT scanner. This (phantom) test should include host and graft bones with different anatomy, a higher number of reconstructions and multiple operators.

Additionally, implementation of this method in a clinical setting involves some challenges, including preoperative imaging of the allograft bone, intraoperative (semi)automatic segmentation of the bone defect and (semi)automatic registration two anatomically different bones (allograft and patient bone).

2.

Based on the experiences to date with the Airo CT scanner in orthopaedic oncology surgery, the Airo CT scanner is considered a substantial improvement. We benefitted especially from:

- Easy, accurate registration on any anatomy
- Visualizing the actual intraoperative anatomy (e.g. for navigation on the spine or screw placement after tumor resection)
- Intraoperative 3D imaging (e.g. for intraoperative screw position verification, making direct revision possible).

However, this comes with the disadvantage of higher patient radiation dose and additional preparation. Also, surgical workflow is obstructed when acquiring a CT scan. However, this was performed in only 3-4 minutes in the last four cases and it is not considered a problem.

7 Recommendations

7.1 Navigated allograft reconstruction

The pilot study included in this thesis has several limitations that are mentioned in the discussion of the article. It is recommended to perform an additional phantom test to further evaluate the potential and challenges of navigated allograft reconstruction in combination with the intraoperative CT scanner. It is recommended that an additional Sawbone study includes:

- Multiple operators
- Sawbones with different anatomy
- More reconstructions per bone defect

It is expected that navigated allograft reconstruction is more accurate in the additional Sawbone test, especially when including Sawbones with different anatomy. Eventually implementing navigated allograft reconstruction using a reconstruction planning made from intraoperative CT in the clinical practice involves several challenges. Regarding navigated allograft reconstruction and its implementation in clinical practice, the following recommendations are made:

Acquiring a CT scan of the allograft

A scan of the allograft has to be available in order to match it with the patient bone. This is the most important challenge because without an allograft scan, the reconstruction planning cannot be used. In summary, the reconstruction planning is made by segmenting the bone defect (the bone defect segmentation is the reconstruction planning) and transferring this reconstruction planning to the allograft scan which is fused for a best fit to the patient bone.

Acquiring the allograft scan can be accomplished in two different ways, each having its advantages and disadvantages:

- Acquire allograft scan preoperatively
- Acquire allograft scan intraoperatively together with the bone defect scan

Acquiring the allograft scan preoperatively involves logistical challenges as the allograft bone is stored in deep freeze. However, acquiring the allograft scan preoperatively gives the surgeon more time to fuse the allograft scan with the patient bone to find the best fit. If the allograft scans are to be acquired preoperatively, methods to scan the allograft bone must be developed, taking logistical challenges and allograft properties (stored in deep freeze) into account.

The allograft bone can also be scanned together with the bone defect, intraoperatively. This means that after the scan is acquired and transported to iPlan, the patient bone and the allograft bone have to be segmented and stored in separate CT scans. Those separate CT scans can then be used to fuse the patient bone with the allograft bone. The reconstruction planning can be made and attached to the allograft scan. An advantage of this method is that the allograft does not have to be outside deep freeze storage before the operation. A disadvantage of this method is that the patient bone with bone defect and the allograft bone have to be segmented and stored in different CT scans, which costs valuable operation time. Additionally, the surgeon will have limited time to determine the image fusion that will result in the best fit, if no automatic algorithms are available.

If no automatic fusion algorithm is present, it is recommended to acquire the allograft bone CT scan preoperatively. OR workflow will then not be further obstructed by the manual image fusion of two anatomically different bones in addition to making the reconstruction planning.

Allograft registration for navigation

In the pilot phantom study, registration of the allograft Sawbone was performed using the Airo CT scanner. However, performing registration for navigation of the allograft bone using the Airo CT would mean additional patient radiation dose. Registration of the allograft bone should therefore be performed using one of the conventional registration methods. Surface matching would be cumbersome as the workflow in the Curve is only suited for registration of vertebras. Fluoro-matching would require an additional device in the OR: the C-arm. Therefore, paired point matching is in this case the best suited conventional registration method. Accurate paired point matching on the allograft bone could for instance be achieved by creating small cortex defects with a drill or by using other markers that are easily identifiable, both on CT imaging and with a navigated pointer.

Making the reconstruction planning

Making the reconstruction planning in the pilot phantom study was not difficult, because segmentation of the Sawbones was performed using a threshold without problems. However, intraoperative patient image data contains blood, soft tissue and absorption materials which all make the (visual) segmentation harder to perform. Completely drawing the reconstruction planning manually will be time consuming. It is therefore recommended to develop (semi-)automatic segmentation methods that can be used intraoperatively. This would benefit OR workflow.

Allograft CT database

When routinely performing navigated allograft reconstruction in combination with the Airo CT scanner it is recommended to create an allograft CT database. More accurate matching algorithms than the current 2D template method can be developed and used, improving the anatomical match between patient bone and allograft bone, thereby potentially improving allograft fit. Allograft bones should be routinely scanned for creation of the database, e.g. after return from the processing facility.

Automatic matching algorithm

An automatic matching algorithm should then be developed to select the best fitting allograft from the allograft CT database. Automatic algorithms are reported to select better fitting allografts compared to manual allograft selection. The automatic algorithm could also be used to match the allograft with the patient bone intraoperatively in order to transfer the reconstruction planning to the allograft CT.

7.2 Use of the Airo CT scanner

Preparation

It is recommended that the operation procedures in which Airo will be used are planned at the start of the day. The night shift can place the scanner in the OR and the radiographer can prepare the scanner early before the patient is ready to be brought in the OR. This will save time as this prevents transportation and preparation of the Airo in-between operations.

Gain calibration

It is recommended that the gain calibration is no longer performed before every operation, as it involves 30 minutes warm-up time and can therefore cause delays in OR workflow. It is recommended to schedule a weekly or two-weekly moment to perform the gain calibration.

Initiation of scan workflow

It is recommended that the feature ‘new Airo scan’ on the Curve is not used. When an Airo scan has to be performed, the workflow on the detachable control module should be started and this workflow will automatically trigger the Curve to prepare for registration for navigation. Using the ‘new Airo scan’ function on the Curve while already performing the workflow on the detachable control module could result in the Curve not recognizing the acquired intraoperative CT scan as a navigated CT scan.

No scanogram

It is recommended to not use the scanogram as this will save time and scan area can mostly be accurately determined using the laser on the scanner. Additionally, it will prevent previously described errors present in the software.

Indications for Airo use

It is recommended that Airo CT scanner will routinely be included in orthopaedic oncology surgeries in which navigation is used (tumor resections in the spine, pelvis and extremities with subsequent reconstruction). Our experiences with the registration method were promising as accurate registration was performed on any anatomy and it is considered a substantial improvement over conventional registration methods. Additionally, the surgeon is able to perform the navigated procedure using image data of the actual current anatomy, rather than relying on preoperative image data. Finally, if screws were used for reconstruction, screw positions can accurately be verified intraoperatively, making direct revision possible. This may reduce additional revision surgeries.

8 References

[1] M. Ieguchi, M. Hoshi, J. Takada, N. Hidaka, and H. Nakamura, “Navigation-assisted surgery for bone and soft tissue tumors with bony extension,” *Clin Orthop Relat Res*, vol. 470, no. 1, pp. 275–283, 2012.

[2] L. E. Ritacco, F. E. Milano, G. L. Farfalli, M. a Ayerza, D. L. Muscolo, and L. a Aponte-Tinao, “Accuracy of 3-D planning and navigation in bone tumor resection.,” *Orthopedics*, vol. 36, no. 7, pp. e942–50, Jul. 2013.

[3] K. C. Wong and S. M. Kumta, “Computer-assisted tumor surgery in malignant bone tumors,” *Clin Orthop Relat Res*, vol. 471, no. 3, pp. 750–761, 2013.

[4] K. C. Wong and S. M. Kumta, “Joint-preserving tumor resection and reconstruction using image-guided computer navigation.,” *Clin. Orthop. Relat. Res.*, vol. 471, no. 3, pp. 762–73, Mar. 2013.

[5] L. Aponte-Tinao, L. E. Ritacco, M. a Ayerza, D. Luis Muscolo, J. I. Albergo, and G. L. Farfall, “Does Intraoperative Navigation Assistance Improve Bone Tumor Resection and Allograft Reconstruction Results?,” *Clin. Orthop. Relat. Res.*, Apr. 2014.

[6] J. Li, Z. Wang, Z. Guo, G.-J. Chen, M. Yang, and G.-X. Pei, “Precise resection and biological reconstruction under navigation guidance for young patients with juxta-articular bone sarcoma in lower extremity: preliminary report,” *J. Pediatr. Oncol.*, vol. 34, no. 1, pp. 101–108, 2014.

[7] L. A. Aponte-Tinao, L. E. Ritacco, M. A. Ayerza, D. L. Muscolo, and G. L. Farfalli, “Multiplanar osteotomies guided by navigation in chondrosarcoma of the knee,” *Orthopedics*, vol. 36, no. 3, pp. e325–30, 2013.

[8] O. Cartiaux, X. Banse, L. Paul, B. G. Francq, C. E. Aubin, and P. L. Docquier, “Computer-assisted planning and navigation improves cutting accuracy during simulated bone tumor surgery of the pelvis,” *Comput Aided Surg*, vol. 18, no. 1–2, pp. 19–26, 2013.

[9] O. Cartiaux, L. Paul, P.-L. Docquier, B. Raucent, E. Dombre, and X. Banse, “Computer-assisted and robot-assisted technologies to improve bone-cutting accuracy when integrated with a freehand process using an oscillating saw.,” *J. Bone Joint Surg. Am.*, vol. 92, no. 11, pp. 2076–82, Sep. 2010.

[10] H. S. Cho, J. H. Oh, I. Han, and H. S. Kim, “Joint-preserving limb salvage surgery under navigation guidance,” *J Surg Oncol*, vol. 100, no. 3, pp. 227–232, 2009.

[11] K. C. Wong, S. M. Kumta, K. H. Chiu, G. E. Antonio, P. Unwin, and K. S. Leung, “Precision tumour resection and reconstruction using image-guided computer navigation.,” *J. Bone Joint Surg. Br.*, vol. 89, no. 7, pp. 943–7, Jul. 2007.

[12] T. Y. C. So, Y.-L. Lam, and K.-L. Mak, “Computer-assisted navigation in bone tumor surgery: seamless workflow model and evolution of technique.,” *Clin. Orthop. Relat. Res.*, vol. 468, no. 11, pp. 2985–91, Nov. 2010.

[13] P.-L. Docquier, L. Paul, O. Cartiaux, C. Delloye, and X. Banse, "Computer-assisted resection and reconstruction of pelvic tumor sarcoma.," *Sarcoma*, vol. 2010, Jan. 2010.

[14] A. Lall, E. Hohn, M. Y. Kim, R. G. Gorlick, J. A. Abraham, and D. S. Geller, "Comparison of Surface Area across the Allograft-Host Junction Site Using Conventional and Navigated Osteotomy Technique.," *Sarcoma*, vol. 2012, Jan. 2012.

[15] L. Kindblom, "Bone tumors: epidemiology, classification, pathology," in *Imaging of Bone Tumors and Tumor-Like Lesions*, M. Davies, M. Sundaram, and S. L. J. James, Eds. 2009, pp. 1–15.

[16] A. Freeman, V. Sumathi, and L. Jeys, "Primary malignant tumours of the bone," *Surgery*, vol. 33, no. 1, pp. 26–33, 2015.

[17] L. Mirabello, R. J. Troisi, and S. A. Savage, "Osteosarcoma incidence and survival rates from 1973 to 2004: data from the Surveillance, Epidemiology, and End Results Program.," *Cancer*, vol. 115, no. 7, pp. 1531–43, Apr. 2009.

[18] K. Mangat, L. Jeys, and S. Carter, "Latest developments in limb-salvage surgery in osteosarcoma," *Expert Rev Anticancer Ther.*, pp. 205–215, 2011.

[19] K. C. Wong, S. M. Kumta, G. E. Antonio, and L. F. Tse, "Image fusion for computer-assisted bone tumor surgery.," *Clin. Orthop. Relat. Res.*, vol. 466, no. 10, pp. 2533–41, Oct. 2008.

[20] J. Bloem, H. van der Woude, M. Geirnaerdt, A. Taminiau, P. Hogendoorn, and C. van Rijswijk, "Bone tumors," *Eur. Radiol.*, vol. 10, no. 2, pp. 207–212, 2000.

[21] W. F. Enneking, "An Abbreviated History of Orthopaedic Oncology in North America," *Clin. Orthop. Relat. Res.*, vol. 374, no. 374, pp. 115–124, May 2000.

[22] U. Quint and U. Vanhöfer, "Cytotoxicity of phenol to musculoskeletal tumours," *J Bone Jt. Surg*, pp. 5–6, 1996.

[23] J. Bickels and I. Meller, "The role and biology of cryosurgery in the treatment of bone tumors: a review," *Acta Orthop Scand*, vol. 70, no. 3, pp. 308–315, 1999.

[24] M. J. Klein and G. P. Siegal, "Osteosarcoma," *Am. J. Clin. Pathol.*, vol. 125, no. 4, pp. 555–581, Apr. 2006.

[25] L. H. Aksnes, H. C. F. Bauer, N. L. Jebsen, G. Follerås, C. Allert, G. S. Haugen, and K. S. Hall, "Limb-sparing surgery preserves more function than amputation: a Scandinavian sarcoma group study of 118 patients.," *J. Bone Joint Surg. Br.*, vol. 90, no. 6, pp. 786–94, Jun. 2008.

[26] L. M. Jeys, a Kulkarni, R. J. Grimer, S. R. Carter, R. M. Tillman, and a Abudu, "Endoprosthetic reconstruction for the treatment of musculoskeletal tumors of the appendicular skeleton and pelvis.," *J. Bone Joint Surg. Am.*, vol. 90, no. 6, pp. 1265–71, Jun. 2008.

[27] G. Gosheger, C. Gebert, H. Ahrens, A. Streitbuerger, W. Winkelmann, and J. Hardes, "Endoprosthetic Reconstruction in 250 Patients with Sarcoma," *Clin. Orthop. Relat. Res.*, vol. 450, no. 450, pp. 164–171, Sep. 2006.

[28] A. Zaretski, A. Amir, I. Meller, D. Leshem, Y. Kollender, Y. Barnea, J. Bickels, T. Shpitzer, D. Ad-El, and E. Gur, "Free Fibula Long Bone Reconstruction in Orthopedic Oncology: A Surgical Algorithm for Reconstructive Options," *Plast. Reconstr. Surg.*, vol. 113, no. 7, pp. 1989–2000, Jun. 2004.

[29] M. P. A. Bus, P. D. S. Dijkstra, M. A. J. van de Sande, A. H. M. Taminiau, H. W. B. Schreuder, P. C. Jutte, I. C. M. van der Geest, G. R. Schaap, and J. A. M. Bramer, "Intercalary allograft reconstructions following resection of primary bone tumors: a nationwide multicenter study.," *J Bone Jt. Surg*, vol. 96, no. 4, p. e26, Feb. 2014.

[30] M. Bus and J. Bramer, "Hemicortical Resection and Inlay Allograft Reconstruction for Primary Bone Tumors," *J Bone Jt. Surg*, pp. 738–750, 2015.

[31] H. J. Mankin, M. C. Gebhardt, L. C. Jennings, D. S. Springfield, and W. W. Tomford, "Long-Term Results of Allograft Replacement in the Management of Bone Tumors," *Clin. Orthop. Relat. Res.*, vol. 324, no. 324, pp. 86–97, Mar. 1996.

[32] S. N. Khan, F. P. Cammisa, H. S. Sandhu, A. D. Diwan, F. P. Girardi, and J. M. Lane, "The biology of bone grafting," *J Am Acad Orthop Surg*, vol. 13, no. 1, pp. 77–86, 2005.

[33] P. S. Young, H. Findlay, J. T. S. Patton, and A. Mahendra, "(iii) Computer assisted navigation in musculoskeletal oncology," *Orthop. Trauma*, vol. 28, no. 5, pp. 294–302, Oct. 2014.

[34] D. Cheong and G. Letson, "Computer-assisted navigation and musculoskeletal sarcoma surgery," *Cancer Control*, pp. 171–176, 2011.

[35] R. Ewers, K. Schicho, G. Undt, F. Wanschitz, M. Truppe, R. Seemann, and a Wagner, "Basic research and 12 years of clinical experience in computer-assisted navigation technology: a review.," *Int. J. Oral Maxillofac. Surg.*, vol. 34, no. 1, pp. 1–8, Jan. 2005.

[36] G. Eggers, B. Kress, and J. Mühling, "Automated registration of intraoperative CT image data for navigated skull base surgery.," *Minim. Invasive Neurosurg.*, vol. 51, no. 1, pp. 15–20, Feb. 2008.

[37] G. Eggers, B. Kress, S. Rohde, and J. Mühling, "Intraoperative computed tomography and automated registration for image-guided cranial surgery.," *Dentomaxillofac. Radiol.*, vol. 38, no. 1, pp. 28–33, Jan. 2009.

[38] E. B. Strong and T. T. Tollefson, "Intraoperative use of CT imaging.," *Otolaryngol. Clin. North Am.*, vol. 46, no. 5, pp. 719–32, Oct. 2013.

[39] G. Zheng, J. Kowal, M. a. González Ballester, M. Caversaccio, and L.-P. Nolte, "(i) Registration techniques for computer navigation," *Curr. Orthop.*, vol. 21, no. 3, pp. 170–179, Jun. 2007.

[40] R. Bächler, H. Bunke, and L. Nolte, "Restricted surface matching—numerical optimization and technical evaluation," *Comput. Aided Surg.*, vol. 152, pp. 143–152, 2001.

[41] M. a. Audette, F. P. Ferrie, and T. M. Peters, "An algorithmic overview of surface registration techniques for medical imaging," *Med. Image Anal.*, vol. 4, no. 3, pp. 201–217, Sep. 2000.

[42] P. J. Besl and H. D. McKay, “A method for registration of 3-D shapes,” *IEEE Trans. Pattern Anal. Mach. Intell.*, vol. 14, no. 2, pp. 239–256, 1992.

[43] J. Maintz and M. Viergever, “A survey of medical image registration,” *Med. Image Anal.*, vol. 2, no. 1, pp. 1–36, 1998.

[44] J. M. Fitzpatrick, D. L. G. Hill, and C. R. Maurer, “Image Registration,” in *Handbook of medical imaging. Medical image processing and analysis*, Vol. 2., M. Sonka and J. Fitzpatrick, Eds. Bellingham: SPIE Press, 2000, pp. 447–513.

[45] B. Zitová and J. Flusser, “Image registration methods: a survey,” *Image Vis. Comput.*, vol. 21, no. 11, pp. 977–1000, Oct. 2003.

[46] D. L. G. Hill, P. G. Batchelor, M. Holden, and D. J. Hawkes, “Medical image registration,” *Phys. Med. Biol.*, vol. 46, no. 3, pp. R1–R45, Mar. 2001.

[47] X. Zhang, G. Zheng, F. Langlotz, and L.-P. Nolte, “Assessment of spline-based 2D-3D registration for image-guided spine surgery.,” *Minim. Invasive Ther. Allied Technol.*, vol. 15, no. 3, pp. 193–9, Jan. 2006.

[48] G. Penney and J. Weese, “A comparison of similarity measures for use in 2-D-3-D medical image registration,” *Med. Imaging, IEEE Trans.*, vol. 17, no. 4, pp. 586–595, 1998.

[49] H. Livyatan, Z. Yaniv, and L. Joskowicz, “Gradient-based 2-D/3-D rigid registration of fluoroscopic X-ray to CT,” *Med. Imaging, IEEE Trans.*, vol. 22, no. 11, pp. 1395–1406, 2003.

[50] a Uneri, Y. Otake, a S. Wang, G. Kleinszig, S. Vogt, a J. Khanna, and J. H. Siewerdsen, “3D-2D registration for surgical guidance: effect of projection view angles on registration accuracy.,” *Phys. Med. Biol.*, vol. 59, no. 2, pp. 271–87, Jan. 2014.

[51] W. Birkfellner, M. Figl, J. Kettenbach, J. Hummel, P. Homolka, R. Schernthaner, T. Nau, and H. Bergmann, “Rigid 2D/3D slice-to-volume registration and its application on fluoroscopic CT images,” *Med. Phys.*, vol. 34, no. 1, p. 246, 2007.

[52] S. Klein, M. Staring, K. Murphy, M. A. Viergever, and J. P. W. Pluim, “Elastix: a toolbox for intensity-based medical image registration,” *IEEE Trans. Med. Imaging*, vol. 29, no. 1, pp. 196–205, 2010.

[53] B. Fischer and J. Modersitzki, “A unified approach to fast image registration and a new curvature based registration technique,” *Linear Algebra Appl.*, vol. 380, pp. 107–124, Mar. 2004.

[54] M. Staring, S. Klein, and J. P. W. Pluim, “A rigidity penalty term for nonrigid registration,” *Med. Phys.*, vol. 34, no. 11, p. 4098, 2007.

[55] S. Klein, M. Staring, and J. Pluim, “Evaluation of optimization methods for nonrigid medical image registration using mutual information and B-splines,” *IEEE Trans. Image Process.*, vol. 16, no. 12, pp. 2879–2890, 2007.

[56] S. Klein, J. P. W. Pluim, M. Staring, and M. a. Viergever, “Adaptive Stochastic Gradient Descent Optimisation for Image Registration,” *Int. J. Comput. Vis.*, vol. 81, no. 3, pp. 227–239, Aug. 2008.

[57] P. Picci, L. Sangiorgi, and B. Rougraff, “Relationship of chemotherapy-induced necrosis and surgical margins to local recurrence in osteosarcoma.,” *J. Clin. Oncol.*, vol. 12, no. 12, pp. 2699–2705, 1994.

[58] D. Geller, J. Chan, S. Armstrong, E. Villenueva-Siles, and B. Thornhill, “Joint-preserving wide excision of parosteal osteosarcoma of the proximal humerus using intraoperative navigation: a case report and review of the literature,” *Curr. Orthop. Pract.*, vol. 25, no. 4, pp. 405–409, 2014.

[59] M. Agarwal, A. Puri, C. Anchan, M. Shah, and N. Jambhekar, “Hemicortical excision for low-grade selected surface sarcomas of bone.,” *Clin. Orthop. Relat. Res.*, vol. 459, no. 459, pp. 161–6, Jun. 2007.

[60] J. G. Gerbers, P. M. Van Ooijen, and P. C. Jutte, “Computer-assisted surgery for allograft shaping in hemicortical resection: a technical note involving 4 cases.,” *Acta Orthop.*, vol. 84, no. 2, pp. 224–6, Apr. 2013.

[61] R. P. J. van den Ende and P. D. S. Dijkstra, “Knee joint-preservation by inlay allograft reconstruction of the distal femur after resection of osteosarcoma using intraoperative navigation and intraoperative CT: a case report,” 2015.

[62] L. Aponte-Tinao, G. L. Farfalli, L. E. Ritacco, M. a Ayerza, and D. L. Muscolo, “Intercalary femur allografts are an acceptable alternative after tumor resection.,” *Clin. Orthop. Relat. Res.*, vol. 470, no. 3, pp. 728–34, Mar. 2012.

[63] D. L. Muscolo, M. a Ayerza, L. Aponte-Tinao, M. Ranalletta, and E. Abalo, “Intercalary Femur and Tibia Segmental Allografts Provide an Acceptable Alternative in Reconstructing Tumor Resections,” *Clin. Orthop. Relat. Res.*, vol. 426, no. 426, pp. 97–102, Sep. 2004.

[64] Z. Wu, J. Fu, Z. Wang, X. Li, J. Li, Y. Pei, G. Pei, D. Li, Z. Guo, and H. Fan, “Three-dimensional virtual bone bank system for selecting massive bone allograft in orthopaedic oncology.,” *Int. Orthop.*, vol. 39, no. 6, pp. 1151–8, Jun. 2015.

[65] H.-J. Jung, G. Vangipuram, M. B. Fisher, G. Yang, S. Hsu, J. Bianchi, C. Ronholdt, and S. L.-Y. Woo, “The effects of multiple freeze-thaw cycles on the biomechanical properties of the human bone-patellar tendon-bone allograft.,” *J. Orthop. Res.*, vol. 29, no. 8, pp. 1193–8, Aug. 2011.

[66] J. M. Shaw, S. a Hunter, J. C. Gayton, G. P. Boivin, and M. J. Prayson, “Repeated freeze-thaw cycles do not alter the biomechanical properties of fibular allograft bone.,” *Clin. Orthop. Relat. Res.*, vol. 470, no. 3, pp. 937–43, Mar. 2012.

[67] L. Paul, P.-L. Docquier, O. Cartiaux, O. Cornu, C. Delloye, and X. Banse, “Selection of massive bone allografts using shape-matching 3-dimensional registration.,” *Acta Orthop.*, vol. 81, no. 2, pp. 250–5, Apr. 2010.

[68] L. E. Ritacco, A. A. Espinoza Orías, L. Aponte-Tinao, D. L. Muscolo, F. G. B. De Quirós, and I. Nozomu, "Three-dimensional morphometric analysis of the distal femur: A validity method for allograft selection using a virtual bone bank," in *Studies in Health Technology and Informatics*, 2010, vol. 160, no. PART 1, pp. 1287–1290.

[69] L. Paul, P.-L. Docquier, O. Cartiaux, O. Cornu, C. Delloye, and X. Banse, "Inaccuracy in selection of massive bone allograft using template comparison method.," *Cell Tissue Bank.*, vol. 9, no. 2, pp. 83–90, Jun. 2008.

[70] H. Bousleiman, L. Paul, L.-P. Nolte, and M. Reyes, "Comparative evaluation of pelvic allograft selection methods.," *Ann. Biomed. Eng.*, vol. 41, no. 5, pp. 931–8, May 2013.

[71] L. E. Ritacco, G. L. Farfalli, F. E. Milano, M. A. Ayerza, D. L. Muscolo, and L. Aponte-Tinao, "Three-dimensional virtual bone bank system workflow for structural bone allograft selection: a technical report.," *Sarcoma*, vol. 2013, p. 524395, Jan. 2013.

[72] D. Brenner and R. Doll, "Cancer risks attributable to low doses of ionizing radiation: assessing what we really know," *Proc Natl Acad Sci USA*, vol. 100, no. 24, pp. 3–8, 2003.

[73] B. A. Ulsh, "Are Risks from Medical Imaging Still too Small to be Observed or Nonexistent?," *Dose-Response*, vol. 13, no. 1, pp. 1–27, Jan. 2015.

[74] S. Mattsson and M. Nilsson, "On the estimation of radiation-induced cancer risks from very low doses of radiation and how to communicate these risks.," *Radiat. Prot. Dosimetry*, vol. 165, no. 1–4, pp. 17–21, 2015.

[75] G. Bongartz, S. Golding, A. Jurik, M. Leonardi, E. Persijn van Meerten, R. Rodriguez, K. Schneider, A. Calzado, J. Geleijns, K. Jessen, W. Panzer, P. Shrimpton, and G. Tosi, "European guidelines for multislice computed tomography. Funded by the European Commission.," 2004, Contract number: FIGMCT2000-20078-CT-TIP

[76] C.-Y. Lee, M.-H. Wu, Y.-Y. Li, C.-C. Cheng, C.-H. Hsu, T.-J. Huang, and R. W.-W. Hsu, "Intraoperative computed tomography navigation for transpedicular screw fixation to treat unstable thoracic and lumbar spine fractures: clinical analysis of a case series (CARE-compliant).," *Medicine (Baltimore).*, vol. 94, no. 20, p. e757, May 2015.

[77] N. Bronsard, T. Boli, M. Challali, R. de Dompsure, N. Amoretti, B. Padovani, G. Bruneton, a Fuchs, and F. de Peretti, "Comparison between percutaneous and traditional fixation of lumbar spine fracture: intraoperative radiation exposure levels and outcomes.," *Orthop. Traumatol. Surg. Res.*, vol. 99, no. 2, pp. 162–8, Apr. 2013.

[78] J. Villard, Y.-M. Ryang, A. K. Demetriades, A. Reinke, M. Behr, A. Preuss, B. Meyer, and F. Ringel, "Radiation exposure to the surgeon and the patient during posterior lumbar spinal instrumentation: a prospective randomized comparison of navigated versus non-navigated freehand techniques.," *Spine (Phila. Pa. 1976).*, vol. 39, no. 13, pp. 1004–9, Jun. 2014.

[79] U. Berlemann, P. Heini, and U. Müller, "Reliability of pedicle screw assessment utilizing plain radiographs versus CT reconstruction," *Eur. spine J.*, pp. 406–410, 1997.

9 Appendices

9.1 Appendix A: Analysis of allograft fit, elastix parameters

9.1.1 Appendix A1: Rigid registrations – Sawbone scans

```
// **************** Main Components **************************
(FixedInternalImagePixelType "float")
(MovingInternalImagePixelType "float")
(FixedImageDimension 3)
(MovingImageDimension 3)
(UseDirectionCosines "true")

// ***************** Transformation **************************
(Transform "EulerTransform")
(AutomaticScalesEstimation "true")
(AutomaticTransformInitialization "true")
(HowToCombineTransforms "Compose")

// ******************* Similarity measure ********************
(Metric "AdvancedMattesMutualInformation")
(NumberOfHistogramBins 32)
(ErodeMask "false")
(RequiredRatioOfValidSamples 0.05)

// ******************** Multiresolution **********************
(Registration "MultiResolutionRegistration")
(NumberOfResolutions 3)
(FixedImagePyramid "FixedRecursiveImagePyramid")
(MovingImagePyramid "MovingRecursiveImagePyramid")

// ******************* Optimizer *****************************
(Optimizer "AdaptiveStochasticGradientDescent")
(MaximumNumberOfIterations 1000)
(MaximumStepLength 1.0)

// **************** Image sampling ***************************
(NumberOfSpatialSamples 2048)
(NewSamplesEveryIteration "true")
(ImageSampler "Random")

// ************* Interpolation and Resampling ****************
(Interpolator "BSplineInterpolator")
(Resampler "DefaultResampler")
(ResampleInterpolator "FinalBSplineInterpolator")
(BSplineInterpolationOrder 1)
(FinalBSplineInterpolationOrder 3)

(DefaultPixelValue 0)
(WriteResultImage "true")
(ResultImagePixelType "short")
(ResultImageFormat "mhd")
```

9.1.2 Appendix A2: Rigid registrations – atlases

```
// **************** Main Components **************************
(FixedInternalImagePixelType "float")
(MovingInternalImagePixelType "float")
(FixedImageDimension 3)
(MovingImageDimension 3)
(UseDirectionCosines "true")

// ***************** Transformation **************************
(Transform "EulerTransform")
(AutomaticScalesEstimation "true")
(AutomaticTransformInitialization "true")
(HowToCombineTransforms "Compose")

// ******************* Similarity measure ********************
(Metric "AdvancedMattesMutualInformation")
(NumberOfHistogramBins 32)
(ErodeMask "false")
(RequiredRatioOfValidSamples 0.05)

// ******************** Multiresolution **********************
(Registration "MultiResolutionRegistration")
(NumberOfResolutions 3)
(FixedImagePyramid "FixedRecursiveImagePyramid")
(MovingImagePyramid "MovingRecursiveImagePyramid")

// ******************* Optimizer *****************************
(Optimizer "AdaptiveStochasticGradientDescent")
(MaximumNumberOfIterations 1000)
(MaximumStepLength 1.0)

// **************** Image sampling ***************************
(NumberOfSpatialSamples 2048)
(NewSamplesEveryIteration "true")
(ImageSampler "Random")

// ************* Interpolation and Resampling ****************
(Interpolator "BSplineInterpolator")
(Resampler "DefaultResampler")
(ResampleInterpolator "FinalBSplineInterpolator")
(BSplineInterpolationOrder 1)
(FinalBSplineInterpolationOrder 0)

(DefaultPixelValue 0)
(WriteResultImage "true")
(ResultImagePixelType "short")
(ResultImageFormat "mhd")
```

9.1.3 Appendix A3: Non-rigid registration – atlas

```
// **************** Main Components **************************
(FixedInternalImagePixelType "float")
(MovingInternalImagePixelType "float")
(FixedImageDimension 3)
(MovingImageDimension 3)
(UseDirectionCosines "true")

// ***************** Transformation **************************
(Transform "BSplineTransform")
(AutomaticScalesEstimation "true")
(AutomaticTransformInitialization "true")
(HowToCombineTransforms "Compose")

// ******************* Similarity measure ********************
(Metric "NormalizedMutualInformation")
(NumberOfHistogramBins 32)
(ErodeMask "false")
(RequiredRatioOfValidSamples 0.05)

// ******************** Multiresolution **********************
(Registration "MultiResolutionRegistration")
(NumberOfResolutions 3)
(FixedImagePyramid "FixedRecursiveImagePyramid")
(MovingImagePyramid "MovingRecursiveImagePyramid")

// ******************* Optimizer *****************************
(Optimizer "AdaptiveStochasticGradientDescent")
(MaximumNumberOfIterations 1000)
(MaximumStepLength 1.0)

// **************** Image sampling ***************************
(NumberOfSpatialSamples 2000)
(NewSamplesEveryIteration "true")
(ImageSampler "Grid")

// ************* Interpolation and Resampling ****************
(Interpolator "BSplineInterpolator")
(Resampler "DefaultResampler")
(ResampleInterpolator "FinalBSplineInterpolator")
(BSplineInterpolationOrder 1)
(FinalBSplineInterpolationOrder 0)

(DefaultPixelValue 0)
(WriteResultImage "true")
(ResultImagePixelType "short")
(ResultImageFormat "mhd")
```

9.2 Appendix B: OR setups

Appendix B1 and B2 contain the OR setups for head first procedures and a feet first procedures, respectively.

Displayed in the OR setup image:

- Airo and integrated table system (black)
- Patient (blue)
- Operator (Op)
- Instrument assistant (Ins)
- Operator assistant (Aio)
- Assistant (As)
- Anesthesiologist (An)
- Curve system (green)
- Infrafred camera (C) (green)
- Surgical instruments (purple)
- Anesthesiologist hardware (red)
- Lead glass panels (yellow)

9.2.1 Appendix B1: OR setup, head first

This OR setup is used during operation procedures on low-thoracic spine, lumbar spine, pelvis, sacrum and upper extremities. During the scan procedure, the operator, instrument assistant and operator assistant will move behind the large lead glass panel. The anesthesiologist, assistant and radiographer will move behind the small lead glass panel.

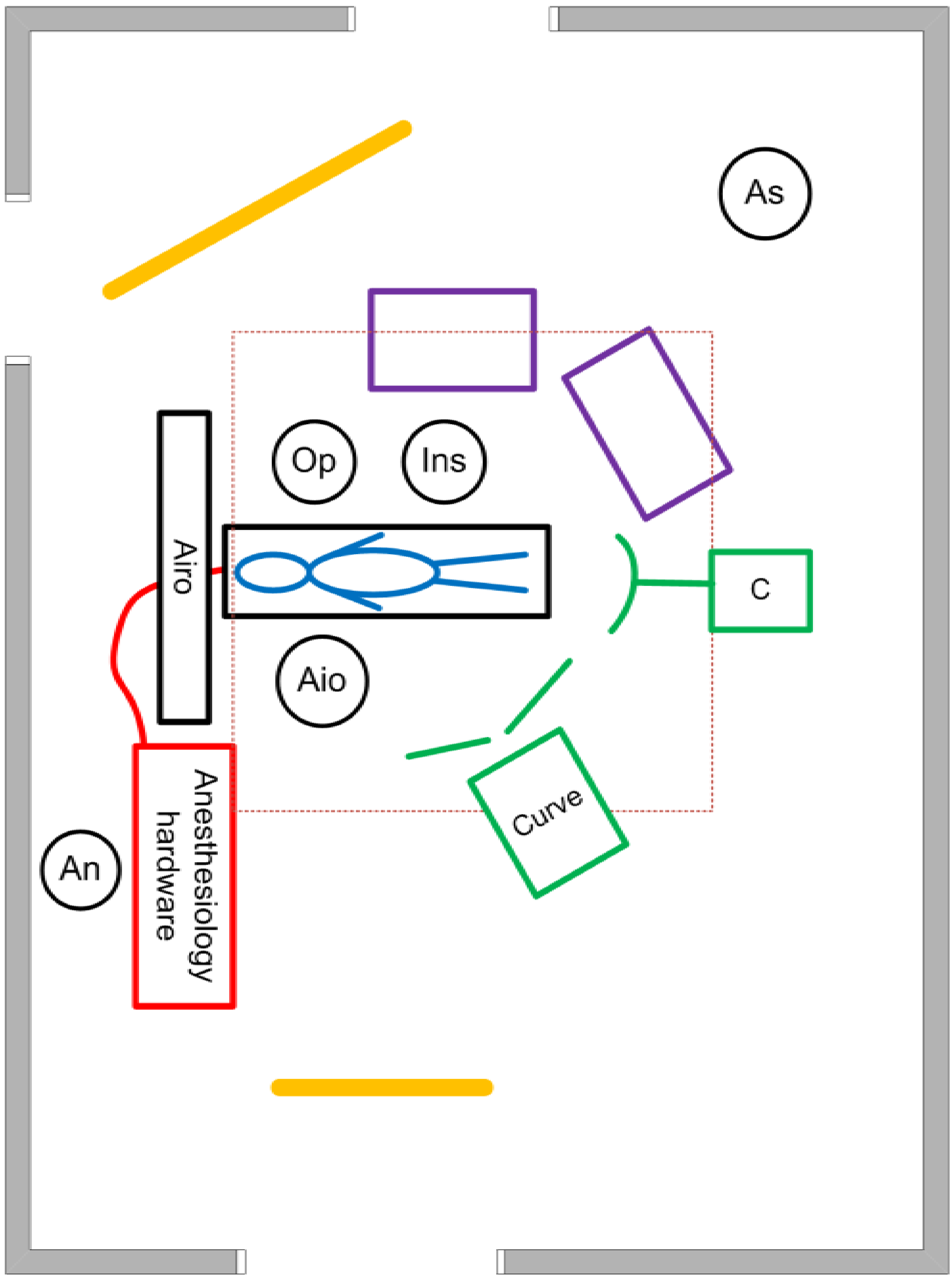

9.2.2 Appendix B2: OR setup, feet first

This OR setup is used during operation procedures on pelvis, sacrum and lower extremities. During the scan procedure, the operator, instrument assistant and operator assistant will move behind the large lead glass panel. The anesthesiologist, assistant and radiographer will move behind the small lead glass panel.

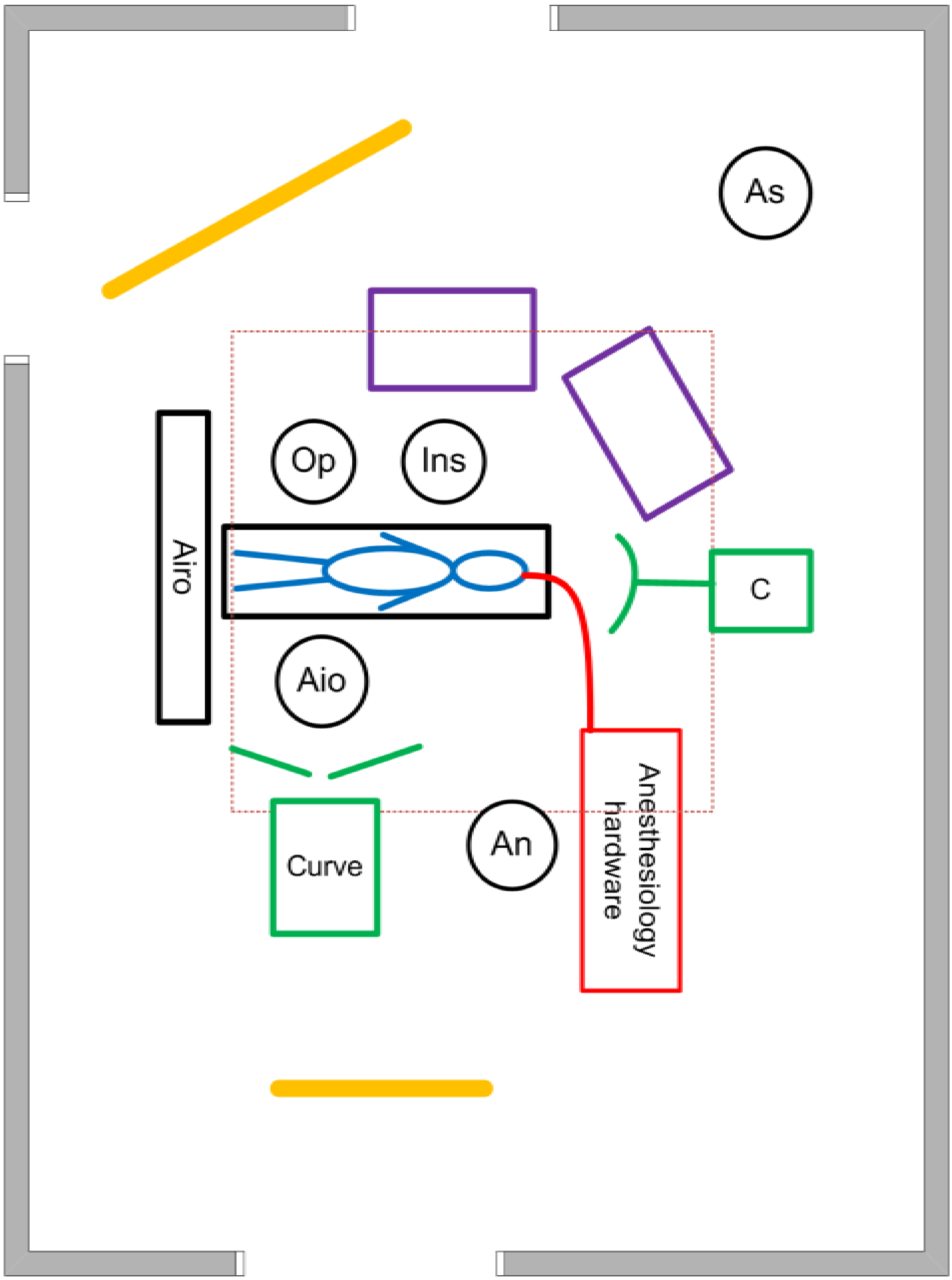

9.3 Appendix C: Workflows navigated procedure

In appendix C1, the preparation for any navigated procedure, regardless of registration method, is shown. The orange blocks represent the different registration methods, with each their own workflow, shown in appendix C2 to C5.

In the workflows, the shape of each block defines its type:

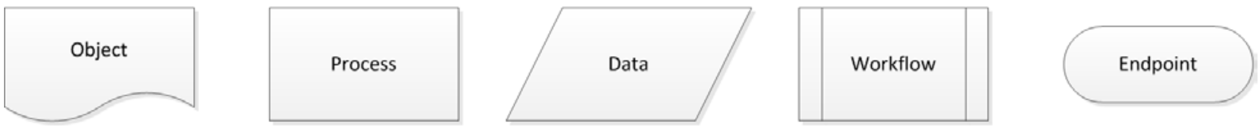

Several preparations are mentioned. Short descriptions of these preparations are given below:

Preparation curve
The preparation of the curve involves connecting power supply and ground cable, booting it and loading preoperative patient data by connecting it to the hospital network using an UTP cable.

Preparation infrared camera
Preparation of the infrared camera involves placing it in a suitable spot within the OR and connecting it to the Curve.

Preparation Airo
Preparation of the Airo involves:

- Transport from storage to the OR
- Correct positioning in the OR
- Lowering the system onto the floor
- Rotating the gantry in the appropriate direction (gantry markers facing the camera)
- Connecting power supply and ground cable
- Connecting UTP cable to the Curve
- Connecting UTP cable to hospital network
- Performing an emergency stop test, warm-up scan and gain calibration (if indicated)
- Mounting the patient table
- Retrieving patient data from the hospital network

Preparation fluoroscopy device
Preparation of the fluoroscopy device involves:

- Transportation from storage to the OR
- Connecting power supply and ground cable
- Connecting communication cable to Curve

9.3.1 Appendix C1: General navigation preparation

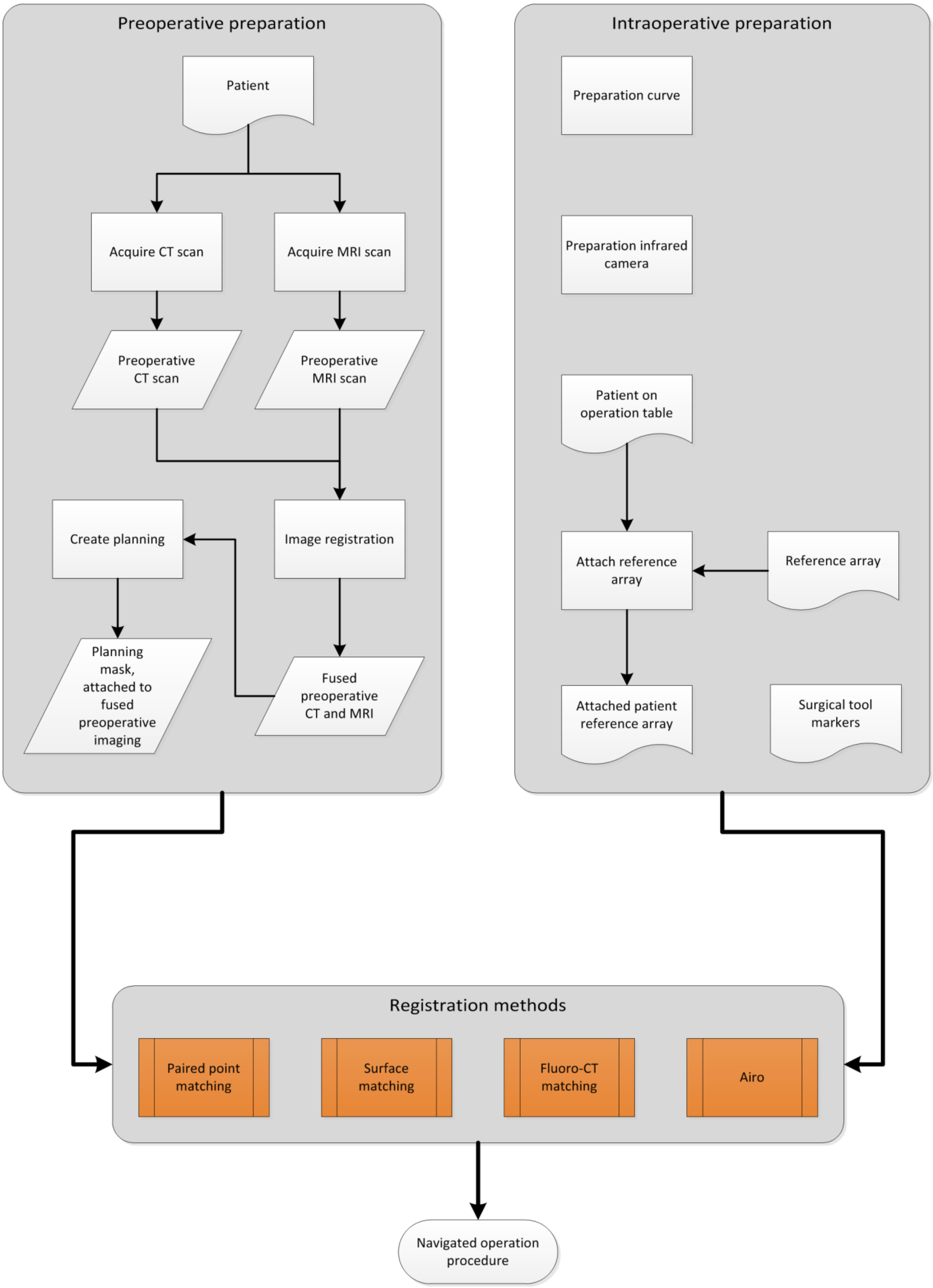

9.3.2 Appendix C2: Registration workflow paired point matching

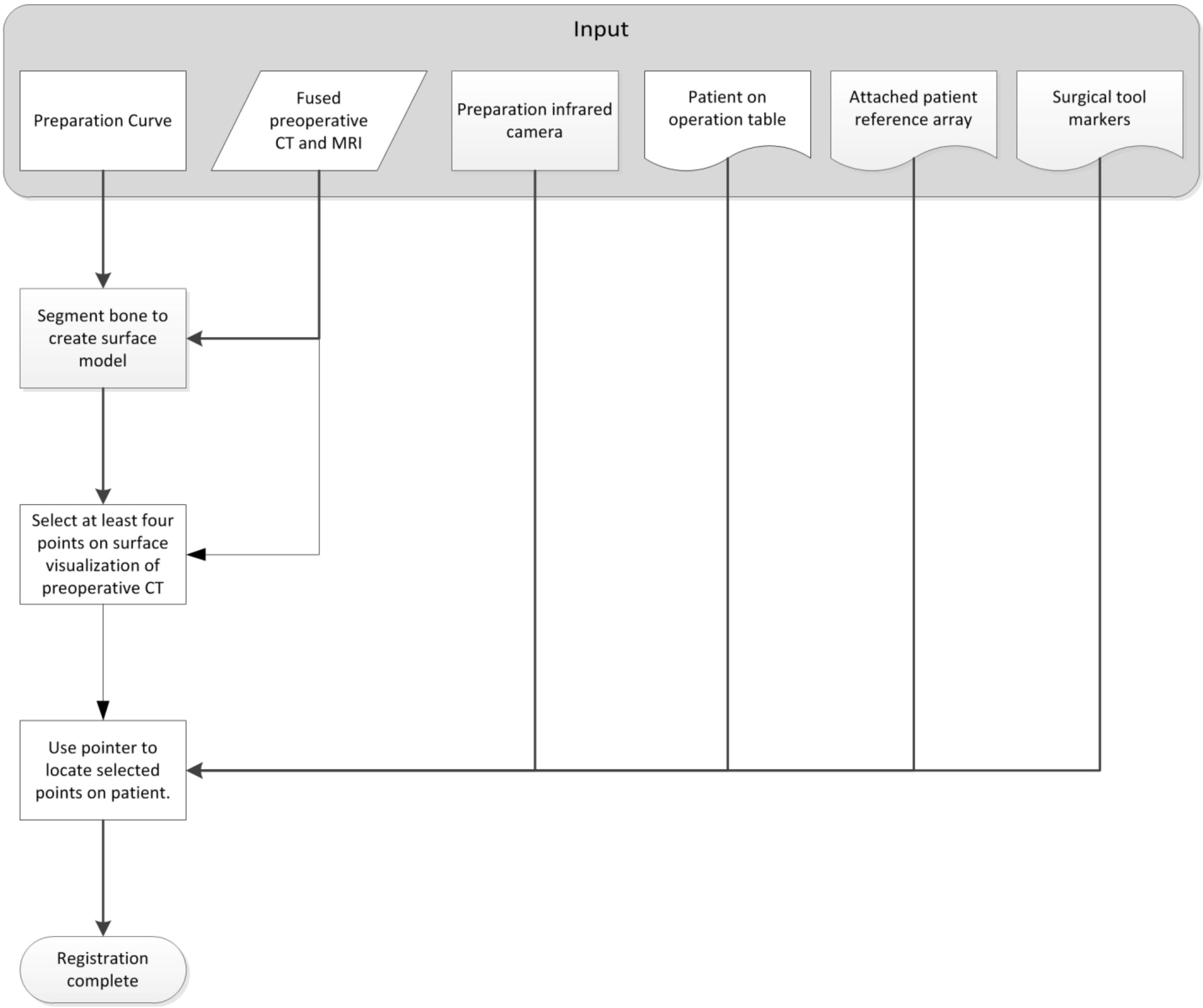

9.3.3 Appendix C3: Registration workflow surface matching

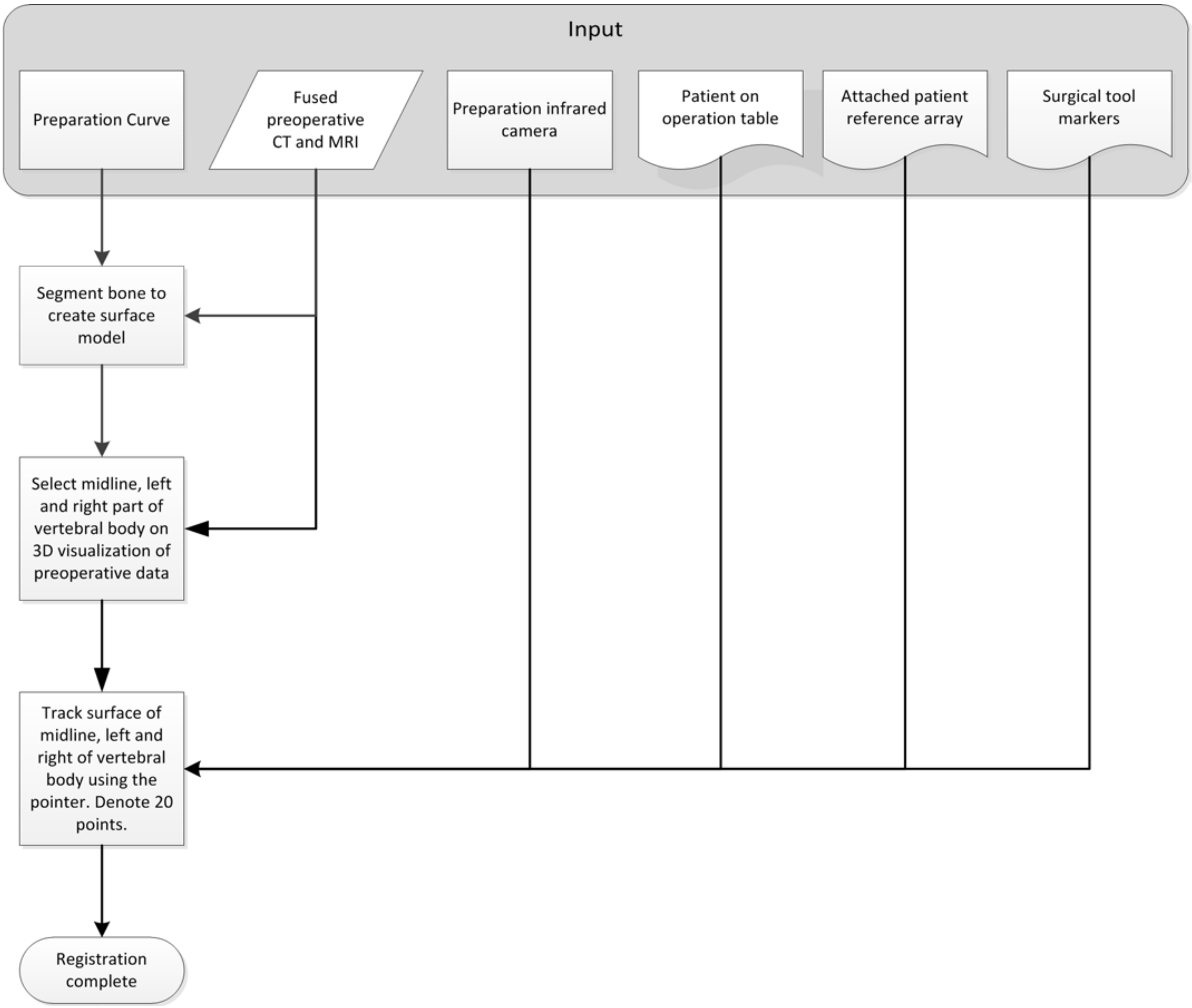

9.3.4 Appendix C4: Registration workflow fluoro-CT matching

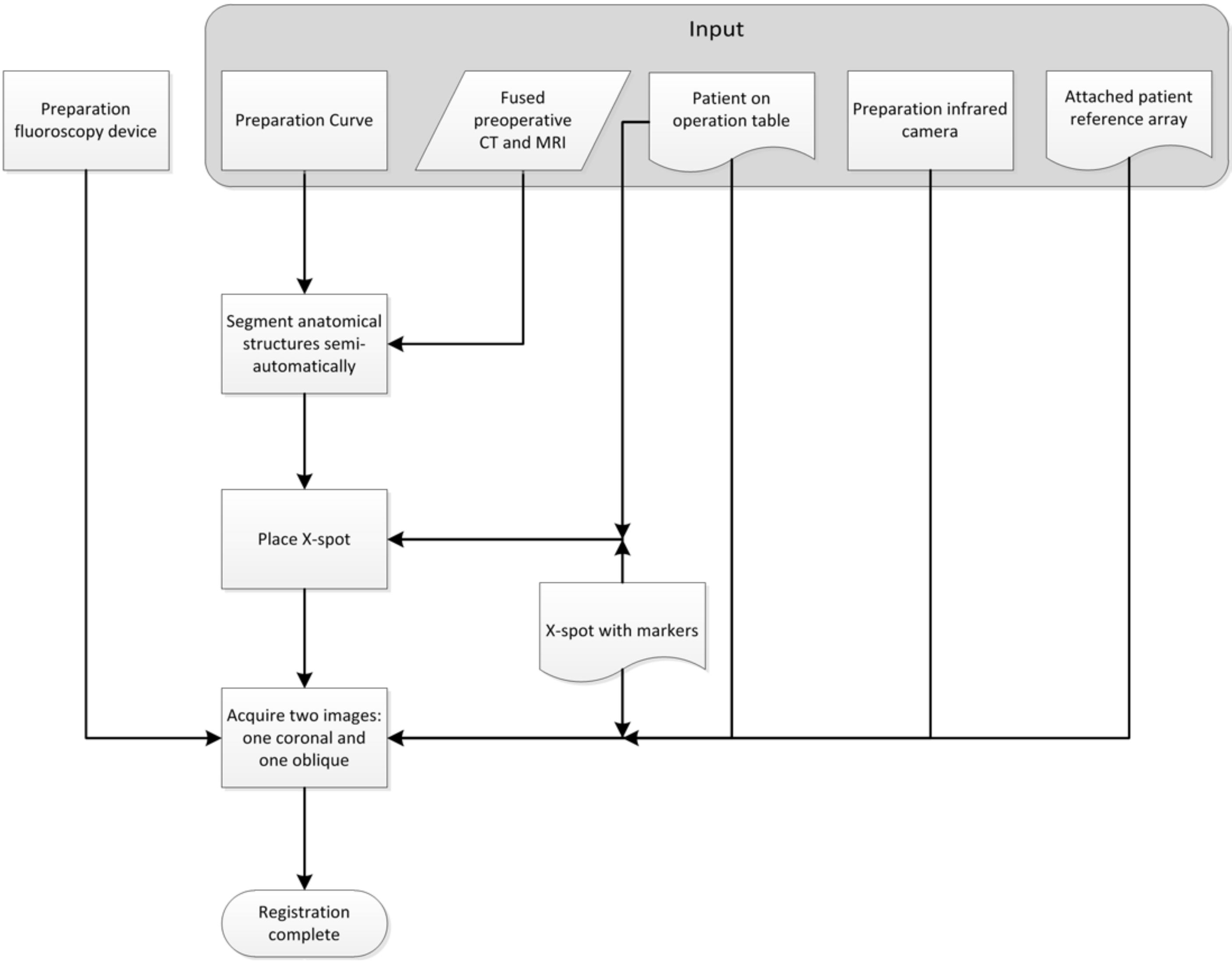

9.3.5 Appendix C5: Registration workflow Airo